Mechanism and Machine Theory 196 (2024) 105613

Contents lists available at ScienceDirect

Mechanism and Machine Theory

journal homepage: www.elsevier.com/locate/mechmt

Research paper

Kinematic jerk and jounce for multibody dynamics with joint constraints

H.J. Sommer III

Mechanical Engineering, The Pennsylvania State University, University Park, PA 16802 USA

ARTICLE INFO

Keywords:
Jerk
Jounce
Planar
Spatial
Multibody dynamics

ABSTRACT

Planar and spatial joint constraint equations for jerk and jounce were derived for multibody dynamics. Exemplar derivations are provided. Results from kinematically driven numerical simulations of these new equations were compared to explicit geometric solutions for planar four-bar and inverted slider-crank mechanisms as well as spatial revolute-spherical-universal-revolute and revolute-spherical-prismatic-universal mechanisms. Root-mean-square-error between velocity, acceleration, jerk and jounce simulations versus explicit solutions were normalized by maximum absolute values for comparison. Relative precisions for new jerk and jounce computations were equivalent to relative precisions for extant velocity and acceleration computations. The new equations were significantly more accurate than finite difference approximations previously required for jerk and jounce. Third and fourth order kinematics developed for this paper are required to explore hyper-dynamic differential algebraic equations created by first and second derivatives of equations of motion for multibody systems using joint constraint methods.

1. Introduction

Kinematic jerk is the third time derivative of position and the first time derivative of acceleration. Consequently, jerk in multibody dynamics is related to magnitude of force transients that may saturate actuator slew rates, excite vibrations, and propagate acoustic noise. Similarly, jounce (also called snap or hyper-jerk) is the fourth derivative of position and the second derivative of acceleration. Jounce is related to frequency content of force transients. The fifth derivative of position is called crackle and the sixth derivative is called pop.

Hayati, et al. [1] provide an interesting review of jerk applied to a wide variety of fields in science and engineering. Historically in mechanism and machine theory, motion trajectories of cam-follower systems [2] were designed to minimize jerk and reduce contact wear and vibration. More recently, this concept of minimum jerk has been extended to planning motion trajectories for robotic manipulators [3–9], computer-controlled machining [10–13], unmanned aircraft [14–16], and unmanned ground vehicles [17–18]. Additionally, several of these references have extended the concept to minimizing jounce trajectories. Moonie and Johnson [15] planned minimum pop trajectories for unmanned aircraft carrying slung loads.

In a similar context, Flash and Hogan [19] demonstrated that humans innately attempt to minimize jerk when moving their limbs. Experimental measurement of jerk has been correlated to human movement impairment due to stroke [20–21] and fatigue [22].

Abbreviations: ADL, activities of daily living; DAE, differential algebraic equations; DOF, degrees of freedom; EOM, equations of motion; FD, finite difference; RHS, right-hand-side; RMSE, root-mean-square error; RSPU, revolute-spherical-prismatic-universal; RSSR, revolute-spherical-spherical-revolute; RSUR, revolute-spherical-universal-revolute.

E-mail address: anvilus9@gmail.com.

https://doi.org/10.1016/j.mechmachtheory.2024.105613
Received 13 December 2023; Received in revised form 1 February 2024; Accepted 17 February 2024
Available online 1 March 2024

Jounce has also been used for analysis of handwriting [23] and arm reaching tasks [24]. Lastly, Saho, et al. [25] have shown that deficits in neurological and cognitive function can be identified by anomalous variations in velocity, acceleration, jerk, jounce and crackle of limb segments during activities of daily living (ADL) such as walking, standing and sit-to-stand movements.

Planar analysis of jerk in mechanisms and machines traditionally used vector loop methods [26] and was recently extended to jounce by Figliolini and Lanni [27]. Spatial analysis of jerk and jounce has generally focused on screw methods [28–32], Lie theory [33], dual numbers [34–36] and incipient motion technique [37]. Denavit-Hartenberg matrix methods were used to compute spatial jerk of closed chains by Sommer [38] and to compute generalized force derivatives for open chains by Lo Bianco [39]. Urbinati and Pennestri [40] introduced general jerk analyses for spatial mechanisms based on constraint methods of Haug [41] but did not provide explicit jerk constraints and did not address jounce.

Recently there has been growing interest in computing the first derivative of force for robotics [39], biomechanics [42] and controls [43] as well as first and second derivatives of force for robotics [44]. To this end, several studies discussed the first derivative of equations of motion (EOM) for improved integration of planar multibody systems [45] and for analysis of spatial robotics [46–47]. Several authors [48–49] have also explored the second derivative of EOM using screw mechanics.

To this end, the goal of this paper is to promote use of first and second derivatives of dynamics by extending the joint constraint kinematic methods of Haug, Urbinati and Pennestri. Specific goals are to develop and validate both planar and spatial jerk and jounce kinematics. These new equations will augment current dynamic methods commonly used in commercial simulation packages to allow efficient computation of derivatives of force and help improve forward time integration.

2. General kinematic constraints

Position, velocity and acceleration kinematics for multibody dynamics presented by Haug [41] are shown in (1–3). A nomenclature section is provided in Appendix B for readers who are not familiar with Haug's notation. For *nb* number of moving bodies, the generalized coordinates vector $\mathbf{q}$ will have row order $nq=3\ nb$ for planar motion and row order $nq=6\ nb$ for spatial motion. The constraint vector $\mathbf{\Phi}$ has row order *nc* and contains *nk* number of kinematic joint constraint equations describing how mechanical joints restrict degrees of freedom (DOF) and *nd* number of driver constraint equations which drive remaining free mobility of the mechanism where $nc=nk+nd$. Jacobian $\mathbf{\Phi_q}$ has order *nc x nq* and denotes partial derivatives of constraints $\mathbf{\Phi}$ with respect to generalized coordinates $\mathbf{q}$. For kinematically driven inverse dynamics, $nc=nq$ to permit inversion of $\mathbf{\Phi_q}$and direct solution of (2–3) for $\dot{\mathbf{q}}$ and $\ddot{\mathbf{q}}$. Forward dynamics allows $nc<nq$. Velocity (2) and acceleration (3) equations are respectively first and second time derivatives of constraint Eq. (1) using the chain rule.

$$\mathbf{\Phi}=\mathbf{0} \tag{1}$$

$$\mathbf{\Phi_q}\dot{\mathbf{q}}=\nu \qquad \nu\equiv-\mathbf{\Phi_t} \tag{2}$$

$$\mathbf{\Phi_q}\ddot{\mathbf{q}}=\gamma \qquad \gamma\equiv-\left(\mathbf{\Phi_q}\dot{\mathbf{q}}\right)_\mathbf{q}\dot{\mathbf{q}}-2\mathbf{\Phi_{qt}}\dot{\mathbf{q}}-\mathbf{\Phi_{tt}} \tag{3}$$

The general jerk equation reported by Urbinati and Pennestri [40] is the first time derivative of (3) and is provided in (4). The general jounce equation developed for this paper is the second time derivative of (3) and is shown in (5). These equations are valid for both planar and spatial methods and are valid for both open and closed kinematic chains. These equations are only valid for holonomic constraints. It is important to note that velocity, acceleration, jerk and jounce all use the same Jacobian $\mathbf{\Phi_q}$.

$$\begin{aligned}&\dddot{\mathbf{\Phi}}_\mathbf{q}\dot{\mathbf{q}}=\eta\\&\eta\equiv-3\left(\mathbf{\Phi_q}\dot{\mathbf{q}}\right)_\mathbf{q}\ddot{\mathbf{q}}-\left(\left(\mathbf{\Phi_q}\dot{\mathbf{q}}\right)_\mathbf{q}\dot{\mathbf{q}}\right)_\mathbf{q}\dot{\mathbf{q}}-3\mathbf{\Phi_{qt}}\ddot{\mathbf{q}}-3\left(\mathbf{\Phi_{qt}}\dot{\mathbf{q}}\right)_\mathbf{q}\dot{\mathbf{q}}-3\mathbf{\Phi_{qtt}}\dot{\mathbf{q}}-\mathbf{\Phi_{ttt}}\end{aligned} \tag{4}$$

$$\begin{aligned}&\ddddot{\mathbf{\Phi}}_\mathbf{q}\dot{\mathbf{q}}=\sigma\\&\sigma\equiv-4\left(\mathbf{\Phi_q}\dddot{\mathbf{q}}\right)_\mathbf{q}\dot{\mathbf{q}}-3\left(\mathbf{\Phi_q}\ddot{\mathbf{q}}\right)_\mathbf{q}\ddot{\mathbf{q}}-6\left(\left(\mathbf{\Phi_q}\dot{\mathbf{q}}\right)_\mathbf{q}\ddot{\mathbf{q}}\right)_\mathbf{q}\ddot{\mathbf{q}}-\left(\left(\left(\mathbf{\Phi_q}\dot{\mathbf{q}}\right)_\mathbf{q}\dot{\mathbf{q}}\right)_\mathbf{q}\dot{\mathbf{q}}\right)_\mathbf{q}\dot{\mathbf{q}}\\&\quad-4\mathbf{\Phi_{qt}}\dddot{\mathbf{q}}-12\left(\mathbf{\Phi_{qt}}\dot{\mathbf{q}}\right)_\mathbf{q}\ddot{\mathbf{q}}-4\left(\left(\mathbf{\Phi_{qt}}\dot{\mathbf{q}}\right)_\mathbf{q}\dot{\mathbf{q}}\right)_\mathbf{q}\dot{\mathbf{q}}-6\mathbf{\Phi_{qtt}}\ddot{\mathbf{q}}-6\left(\mathbf{\Phi_{qtt}}\dot{\mathbf{q}}\right)_\mathbf{q}\dot{\mathbf{q}}-4\mathbf{\Phi_{qttt}}\dot{\mathbf{q}}-\mathbf{\Phi_{tttt}}\end{aligned} \tag{5}$$

It should be noted that the jerk right-hand-side (RHS) term η is not simply the time derivative of the acceleration RHS term γ. Similarly, the jounce RHS term σ is not the time derivative of the jerk RHS term. Simplified expressions for acceleration RHS, jerk RHS and jounce RHS are provided in (6–8) for scleronomic constraints that are independent of time such as mechanical joints.

$$\gamma=-\left(\mathbf{\Phi_q}\dot{\mathbf{q}}\right)_\mathbf{q}\dot{\mathbf{q}} \tag{6}$$

$$\eta=\dot{\gamma}-\left(\mathbf{\Phi_q}\ddot{\mathbf{q}}\right)_\mathbf{q}\dot{\mathbf{q}} \tag{7}$$

$$\sigma=\dot{\eta}-\left(\mathbf{\Phi_q}\dddot{\mathbf{q}}\right)_\mathbf{q}\dot{\mathbf{q}} \tag{8}$$

Consequently, kinematics for a given mechanical joint can be represented by a position constraint equation $\mathbf{\Phi^{jnt}}$, respective entries in the kinematic Jacobian $\mathbf{\Phi_q^{jnt}}$, velocity RHS $\nu^{\mathbf{jnt}}$, acceleration RHS $\gamma^{\mathbf{jnt}}$, jerk RHS $\eta^{\mathbf{jnt}}$ and jounce RHS $\sigma^{\mathbf{jnt}}$. Velocity RHS $\nu^{\mathbf{jnt}}$ for a

mechanical joint constraint is zero but velocity RHS $\boldsymbol{\nu}^{\mathbf{dri}}$ for a driver constraint need not be zero.

3. Planar kinematics

Planar position, velocity and acceleration kinematics in (9–12) are presented solely as review for those readers who may not be familiar with Haug [41]. Note that all $\mathbf{s_i}'^{P}$ terms are constant. Jerk (13) was reported by Sommer [45] and jounce (14) was developed specifically for this paper. Relative position, velocity, acceleration and jerk vectors used to form planar joint constraints are provided in (15–20).

$$\mathbf{A_i} = \begin{bmatrix} \cos\phi_i & -\sin\phi_i \\ \sin\phi_i & \cos\phi_i \end{bmatrix} \qquad \mathbf{R} = \begin{bmatrix} 0 & -1 \\ 1 & 0 \end{bmatrix} \qquad \mathbf{B_i} = \mathbf{R}\,\mathbf{A_i} \tag{9}$$

$$\mathbf{r_i^P} = \mathbf{r}_i + \mathbf{A_i}\mathbf{s_i}'^{P} \tag{10}$$

$$\dot{\mathbf{r}}_\mathbf{i}^\mathbf{P} = \dot{\mathbf{r}}_i + \dot{\phi}_i\mathbf{B_i}\mathbf{s_i}'^{P} \tag{11}$$

$$\ddot{\mathbf{r}}_\mathbf{i}^\mathbf{P} = \ddot{\mathbf{r}}_i + \ddot{\phi}_i\mathbf{B_i}\mathbf{s}_i'^{P} - \dot{\phi}_i^{\,2}\mathbf{A_i}\mathbf{s}_i'^{P} \tag{12}$$

$$\dddot{\mathbf{r}}_\mathbf{i}^\mathbf{P} = \dddot{\mathbf{r}}_i + \left(\dddot{\phi}_i - \dot{\phi}_i^{\,3}\right)\mathbf{B_i}\mathbf{s_i}'^{P} - 3\dot{\phi}_i\ddot{\phi}_i\mathbf{A_i}\mathbf{s}_i'^{P} \tag{13}$$

$$\ddddot{\mathbf{r}}_i^{P} = \ddddot{\mathbf{r}}_i + \left(\ddddot{\phi}_{ij} - 6\dot{\phi}_i^2\ddot{\phi}_i\right)\mathbf{B}_i\mathbf{s}_i'^{P} - \left(4\dddot{\phi}_i\dot{\phi}_i + 3\ddot{\phi}_i^2 - \dot{\phi}_i^4\right)\mathbf{A}_i\mathbf{s}_i'^{P} \tag{14}$$

$$\mathbf{d_{ij}} = \mathbf{r_j^P} - \mathbf{r_i^P} = \mathbf{r_j} + \mathbf{A_j}\mathbf{s_j}'^{\mathbf{P}} - \mathbf{r_i} - \mathbf{A_i}\mathbf{s_i}'^{\mathbf{P}} \tag{15}$$

$$\dot{\mathbf{d}}_\mathbf{ij} = \dot{\mathbf{r}}_\mathbf{j}^\mathbf{P} - \dot{\mathbf{r}}_\mathbf{i}^\mathbf{P} = \dot{\mathbf{r}}_\mathbf{j} + \dot{\phi}_j\mathbf{B_j}\mathbf{s_j}'^{\mathbf{P}} - \dot{\mathbf{r}}_\mathbf{i} - \dot{\phi}_i\mathbf{B_i}\mathbf{s_i}'^{\mathbf{P}} \tag{16}$$

$$\ddot{\mathbf{d}}_\mathbf{ij} = \ddot{\mathbf{r}}_\mathbf{j}^\mathbf{P} - \ddot{\mathbf{r}}_\mathbf{i}^\mathbf{P} = \ddot{\mathbf{r}}_\mathbf{j} + \ddot{\phi}_j\mathbf{B_j}\mathbf{s_j}'^{\mathbf{P}} - \dot{\phi}_j^2\mathbf{A_j}\mathbf{s_j}'^{\mathbf{P}} - \ddot{\mathbf{r}}_\mathbf{i} - \ddot{\phi}_i\mathbf{B_i}\mathbf{s_i}'^{\mathbf{P}} + \dot{\phi}_i^2\mathbf{A_i}\mathbf{s_i}'^{\mathbf{P}} \tag{17}$$

$$\dddot{\mathbf{d}}_\mathbf{ij} = \dddot{\mathbf{r}}_\mathbf{j}^\mathbf{P} - \dddot{\mathbf{r}}_\mathbf{i}^\mathbf{P} = \dddot{\mathbf{r}}_j + \left(\dddot{\phi}_j - \dot{\phi}_j^{\,3}\right)\mathbf{B_j}\mathbf{s_j}'^{P} - 3\dot{\phi}_j\ddot{\phi}_j\mathbf{A_j}\mathbf{s_j}'^{\mathbf{PP}} - \dddot{\mathbf{r}}_i - \left(\dddot{\phi}_i - \dot{\phi}_i^{\,3}\right)\mathbf{B_i}\mathbf{s_i}'^{P} + 3\dot{\phi}_i\ddot{\phi}_i\mathbf{A_i}\mathbf{s_i}'^{P} \tag{18}$$

$$\mathbf{a_i} = \mathbf{r_i^Q} - \mathbf{r_i^P} = \mathbf{A_i}\mathbf{a_i}' \tag{19}$$

$$\mathbf{a_i}' = \mathbf{s_i}'^{\mathbf{Q}} - \mathbf{s_i}'^{\mathbf{P}} \tag{20}$$

A planar revolute joint constraint restricts two DOF as shown in (21–23) following Haug [41]. Jerk RHS for a planar revolute joint introduced by Sommer [45] is provided in (24). Jounce RHS developed for this paper is shown in (25). Derivations for jerk and jounce of a planar revolute joint are provided in Appendix A.

$$\mathbf{\Phi^r} = \mathbf{d_{ij}} = \mathbf{r_j^P} - \mathbf{r_i^P} = \mathbf{0} \tag{21}$$

$$\mathbf{\Phi}_\mathbf{qi}^\mathbf{r} = \left[\ -\mathbf{I_2}\ ,\ -\mathbf{B_i}\mathbf{s_i}'^{\mathbf{P}}\ \right] \qquad \mathbf{\Phi}_\mathbf{qj}^\mathbf{r} = \left[\ \mathbf{I_2}\ ,\ \mathbf{B_j}\mathbf{s_j}'^{\mathbf{P}}\ \right] \tag{22}$$

$$\boldsymbol{\gamma}^\mathbf{r} = \dot{\phi}_j^2\mathbf{A_j}\mathbf{s_j}'^{P} - \dot{\phi}_i^2\mathbf{A_i}\mathbf{s_i}'^{P} \tag{23}$$

$$\boldsymbol{\eta}^\mathbf{r} = 3\dot{\phi}_j\ddot{\phi}_j\mathbf{A_j}\mathbf{s_j}'^{P} + \dot{\phi}_j^3\mathbf{B_j}\mathbf{s_j}'^{P} - 3\dot{\phi}_i\ddot{\phi}_i\mathbf{A_i}\mathbf{s_i}'^{P} - \dot{\phi}_i^3\mathbf{B_i}\mathbf{s_i}'^{P} \tag{24}$$

$$\boldsymbol{\sigma}^\mathbf{r} = \left(4\dot{\phi}_j\dddot{\phi}_j + 3\ddot{\phi}_j^2 - \dot{\phi}_j^4\right)\mathbf{A_j}\mathbf{s_j}'^{P} + 6\dot{\phi}_j^2\ddot{\phi}_j\mathbf{B_j}\mathbf{s_j}'^{P} - \left(4\dot{\phi}_i\dddot{\phi}_i + 3\ddot{\phi}_i^2 - \dot{\phi}_i^4\right)\mathbf{A_i}\mathbf{s_i}'^{P} - 6\dot{\phi}_i^2\ddot{\phi}_i\mathbf{B_i}\mathbf{s_i}'^{P} \tag{25}$$

A planar double-revolute joint constraint only restricts one DOF as provided in (26–30). Note that Jacobian, acceleration RHS, jerk RHS and jounce RHS terms utilize corresponding terms from the planar revolute joint for simplification.

$$\Phi^{\mathrm{rr}} = \mathbf{d_{ij}}^{\mathbf{T}}\mathbf{d_{ij}} - L^2 = \left(\mathbf{r_j^P} - \mathbf{r_i^P}\right)^{\mathbf{T}}\left(\mathbf{r_j^P} - \mathbf{r_i^P}\right) - L^2 = 0 \qquad \mathrm{L} = \text{constant length} \tag{26}$$

$$\mathbf{\Phi}^{\mathbf{rr}}_{\mathbf{qi}} = 2\left[\ -\mathbf{d_{ij}}^{\mathbf{T}},\ -\mathbf{d_{ij}}^{\mathbf{T}}\mathbf{B_i}\mathbf{s_i}'^{\mathbf{P}}\ \right] = 2\mathbf{d_{ij}}^{\mathbf{T}}\mathbf{\Phi}^{\mathbf{r}}_{\mathbf{qi}} \qquad \mathbf{\Phi}^{\mathbf{rr}}_{\mathbf{qj}} = 2\left[\ \mathbf{d_{ij}}^{\mathbf{T}},\ \mathbf{d_{ij}}^{\mathbf{T}}\mathbf{B_j}\mathbf{s_j}'^{\mathbf{P}}\ \right] = 2\mathbf{d_{ij}}^{\mathbf{T}}\mathbf{\Phi}^{\mathbf{r}}_{\mathbf{qj}} \tag{27}$$

$$\gamma^{\mathrm{rr}} = 2\mathbf{d_{ij}}^{\mathbf{T}}\boldsymbol{\gamma}^{\mathbf{r}} - 2\dot{\mathbf{d}}_{\mathbf{ij}}^{\mathbf{T}}\dot{\mathbf{d}}_{\mathbf{ij}} \tag{28}$$

$$\eta^{\mathrm{rr}} = -6\dot{\mathbf{d}}_{\mathbf{ij}}^{\mathbf{T}}\ddot{\mathbf{d}}_{\mathbf{ij}} + 2\mathbf{d_{ij}}^{\mathbf{T}}\boldsymbol{\eta}^{\mathbf{r}} \tag{29}$$

$$\sigma^{\mathrm{rr}} = -8\dot{\mathbf{d}}_{ij}^{T}\dddot{\mathbf{d}}_{ij} - 6\ddot{\mathbf{d}}_{ij}^{T}\ddot{\mathbf{d}}_{ij} + 2\mathbf{d}_{ij}^{T}\boldsymbol{\sigma}^{r} \tag{30}$$

A planar prismatic joint restricts two DOF and is constructed by combining the planar parallel-1 and planar parallel-2 constraints below. Planar parallel-1 constraints in (31–33) are equivalent to the second term in Haug's [41] prismatic (translation) constraint. Jerk RHS and jounce RHS in (33) are consistent with a constant relative rotation angle constraint.

$$\Phi^{\mathrm{pp1}} = \mathbf{a_i}^{\mathbf{T}}\mathbf{R}^{\mathbf{T}}\mathbf{a_j} = 0 \tag{31}$$

$$\mathbf{\Phi}^{\mathbf{pp1}}_{\mathbf{qi}} = \left[\ 0\ ,\ 0\ ,\ -\mathbf{a_i}^{\mathbf{T}}\mathbf{a_j}\ \right] \qquad \mathbf{\Phi}^{\mathbf{pp1}}_{\mathbf{qj}} = \left[\ 0\ ,\ 0\ ,\ \mathbf{a_i}^{\mathbf{T}}\mathbf{a_j}\ \right] = -\mathbf{\Phi}^{\mathbf{pp1}}_{\mathbf{qi}} \tag{32}$$

$$\gamma^{\mathrm{pp1}} = 0 \qquad \eta^{\mathrm{pp1}} = 0 \qquad \sigma^{\mathrm{pp1}} = 0 \tag{33}$$

Planar parallel-2 constraints in (34–36) are equivalent to the first term in Haug's [41] prismatic (translation) constraint and provide pin-in-slot motion. Jerk RHS and jounce RHS are provided in (37–38). Jacobian, acceleration RHS, jerk RHS and jounce RHS terms also utilize corresponding terms from the planar revolute joint for simplification.

$$\Phi^{\mathrm{pp2}} = \mathbf{a_i}^{\mathbf{T}}\mathbf{R}^{\mathbf{T}}\mathbf{d_{ij}} = 0 \tag{34}$$

$$\begin{aligned}\mathbf{\Phi}^{\mathbf{pp2}}_{\mathbf{qi}} &= \left[\ -\mathbf{a_i}^{\mathbf{T}}\mathbf{R}^{\mathbf{T}},\ -\mathbf{a_i}^{\mathbf{T}}\mathbf{R}^{\mathbf{T}}\mathbf{B_i}\mathbf{s_i}'^{\mathbf{P}} - \mathbf{a_i}^{\mathbf{T}}\mathbf{d_{ij}}\ \right] = \mathbf{a_i}^{\mathbf{T}}\mathbf{R}^{\mathbf{T}}\mathbf{\Phi}^{\mathbf{r}}_{\mathbf{qi}} - \left[0\ ,\ 0\ ,\ \mathbf{a_i}^{\mathbf{T}}\mathbf{d_{ij}}\right] \\ \mathbf{\Phi}^{\mathbf{pp2}}_{\mathbf{qj}} &= \left[\ \mathbf{a_i}^{\mathbf{T}}\mathbf{R}^{\mathbf{T}},\ \mathbf{a_i}^{\mathbf{T}}\mathbf{R}^{\mathbf{T}}\mathbf{B_j}\mathbf{s_j}'^{\mathbf{P}}\right] = \mathbf{a_i}^{\mathbf{T}}\mathbf{R}^{\mathbf{T}}\mathbf{\Phi}^{\mathbf{r}}_{\mathbf{qj}}\end{aligned} \tag{35}$$

$$\gamma^{\mathrm{pp2}} = \mathbf{a_i}^{\mathbf{T}}\left(2\dot{\phi}_i\dot{\mathbf{d}}_{\mathbf{ij}} + \mathbf{R}^{\mathbf{T}}\left(\dot{\phi}_i^2\mathbf{d_{ij}} + \boldsymbol{\gamma}^{\mathbf{r}}\right)\right) \tag{36}$$

$$\eta^{\mathrm{pp2}} = \mathbf{a_i}^{\mathbf{T}}\left(\left(3\dot{\phi}_i\ddot{\mathbf{d}}_{\mathbf{ij}} + 3\ddot{\phi}_i\dot{\mathbf{d}}_{ij} - \dot{\phi}_i^3\mathbf{d_{ij}}\right) + \mathbf{R}^{\mathbf{T}}\left(3\dot{\phi}_i\ddot{\phi}_i\mathbf{d_{ij}} + 3\dot{\phi}_i^2\dot{\mathbf{d}}_{\mathbf{ij}} + \boldsymbol{\eta}^{\mathbf{r}}\right)\right) \tag{37}$$

$$\sigma^{\mathrm{pp2}} = \mathbf{a_i}^{\mathbf{T}}\left(\begin{array}{l}\left(4\dot{\phi}_i\dddot{\mathbf{d}}_{ij} + 6\ddot{\phi}_i\ddot{\mathbf{d}}_{ij} + 4\left(\dddot{\phi}_i - \dot{\phi}_i^3\right)\dot{\mathbf{d}}_{ij} - 6\dot{\phi}_i^2\ddot{\phi}_i\mathbf{d}_{ij}\right) \\ +\mathbf{R}^{T}\left(6\dot{\phi}_i^2\ddot{\mathbf{d}}_{ij} + 12\dot{\phi}_i\ddot{\phi}_i\dot{\mathbf{d}}_{ij} + \left(4\dot{\phi}_i\dddot{\phi}_i + 3\ddot{\phi}_i^2 - \dot{\phi}_i^4\right)\mathbf{d}_{ij} + \boldsymbol{\sigma}^{r}\right)\end{array}\right) \tag{38}$$

The relative coordinate driver constraint in (39–40) may be used to control absolute location/attitude of a body or relative location/attitude between two bodies. Common applications are $(K = 0)$ for an absolute rotation driver between body j and ground, $(K = 1)$ for a relative rotation driver between two bodies i and j, $(K = \rho,$ *substitute* x_j *or* y_j *for* $\phi_j,\ f(t) = 0)$ for pure rolling of body i with radius $\boldsymbol{\rho}$ in a horizontal/vertical direction, and $(K = -\rho_i/\rho_j,\ f(t) = 0)$ for a gear ratio constraint between two fixed external gears i and j with pitch radii ρ_i and ρ_j. An internal gear pair would have a positive ratio of K. The relative gear ratio constraint between two gears i and j on a rotating frame m required for an epicyclic gear train is provided in (41–43).

$$\Phi^{\mathrm{rcd}} = \phi_j - K\phi_i - C - f(t) = 0 \qquad \mathrm{K = constant,\ C = constant} \tag{39}$$

$$\nu^{\mathrm{rcd}} = \mathrm{f_t} \qquad \gamma^{\mathrm{rcd}} = \mathrm{f_{tt}} \qquad \eta^{\mathrm{rcd}} = \mathrm{f_{ttt}} \qquad \sigma^{\mathrm{rcd}} = \mathrm{f_{tttt}} \tag{40}$$

$$\Phi^{\mathrm{rgr}} = \left(\phi_j - \phi_m\right) - K\left(\phi_i - \phi_m\right) - C = 0 \qquad \mathrm{K = constant,\ C = constant} \tag{41}$$

$$\mathbf{\Phi}^{rgr}_{qi} = [0,\ 0,\ -K] \qquad \mathbf{\Phi}^{rgr}_{qj} = [\ 0,\ 0,\ 1\ ] \qquad \mathbf{\Phi}^{rgr}_{qm} = [\ 0,\ 0,\ K-1\ ] \tag{42}$$

$$\nu^{\mathrm{rgr}} = 0 \qquad \gamma^{\mathrm{rgr}} = 0 \qquad \eta^{\mathrm{rgr}} = 0 \qquad \sigma^{\mathrm{rgr}} = 0 \tag{43}$$

The planar parallel-2 distance driver shown in (44–45) is equivalent to Haug's [41] relative translational driver. Velocity, acceleration, jerk and jounce terms are shown in (46–49). Pure rolling of a wheel with radius ρ along a line can be modelled by adding the relative rotation constraint to the parallel-2 distance driver. The location of the center of the wheel will be related to the rotation between the two bodies as shown in (50–52).

$$\Phi^{\mathrm{pp2dd}} = \mathbf{a}_i^{T}\mathbf{d}_{ij}/L - f(t) = 0 \qquad L = |\mathbf{a}_i| = \text{constant length} \tag{44}$$

$$\mathbf{\Phi}_{qi}^{pp2dd} = \left[\; -\mathbf{a}_i^T, \; -\mathbf{a}_i^T \mathbf{B}_i \mathbf{s}_i^{'P} + \mathbf{a}_i^T \mathbf{R}^T \mathbf{d}_{ij} \; \right] / L \qquad \mathbf{\Phi}_{qj}^{pp2dd} = \left[\; \mathbf{a}_i^T, \; \mathbf{a}_i^T \mathbf{B}_j \mathbf{s}_j^{'P} \; \right] / L \tag{45}$$

$$\nu^{\text{pp2dd}} = \mathrm{f_t} \tag{46}$$

$$\gamma^{\text{pp2dd}} = \mathbf{a}_i^T \left(-2\mathbf{R}^T \dot{\mathbf{d}}_{ij} \dot{\phi}_i + \left(\mathbf{d}_{ij} \dot{\phi}_i^2 + \boldsymbol{\gamma}^{\mathbf{r}} \right) \right) / L + f_{tt} \tag{47}$$

$$\eta^{\text{pp2dd}} = \mathbf{a}_i^T \left(-\mathbf{R}^T \left(3\ddot{\mathbf{d}}_{ij} \dot{\phi}_i + 3\dot{\mathbf{d}}_{ij} \ddot{\phi}_i - \mathbf{d}_{ij} \dot{\phi}_i^3 \right) + \left(3\mathbf{d}_{ij} \dot{\phi}_i \ddot{\phi}_i + 3\dot{\mathbf{d}}_{ij} \dot{\phi}_i^2 + \boldsymbol{\eta}^r \right) \right) / L + f_{ttt} \tag{48}$$

$$\sigma^{\text{pp2dd}} = \mathbf{a}_i^T \begin{pmatrix} -\mathbf{R}^T \left(4\dddot{\mathbf{d}}_{ij} \dot{\phi}_i + 6\ddot{\mathbf{d}}_{ij} \ddot{\phi}_i + 4\dot{\mathbf{d}}_{ij} \left(\dddot{\phi}_i - \dot{\phi}_i^3 \right) - 6\mathbf{d}_{ij} \dot{\phi}_i^2 \ddot{\phi}_i \right) \\ + \left(6\ddot{\mathbf{d}}_{ij} \dot{\phi}_i^2 + 12\dot{\mathbf{d}}_{ij} \dot{\phi}_i \ddot{\phi}_i + \mathbf{d}_{ij} \left(4\dot{\phi}_i \dddot{\phi}_i + 3\ddot{\phi}_i^2 - \dot{\phi}_i^4 \right) + \boldsymbol{\sigma}^r \right) \end{pmatrix} / L + f_{tttt} \tag{49}$$

$$\Phi^{\text{roll}} = \mathbf{a}_i^T \mathbf{d}_{ij} / L - \rho \left(\phi_j - \phi_i \right) - C = 0 \qquad L = |\mathbf{a}_i| = \text{constant}, \; \rho = \text{constant}, \; \mathrm{C} = \text{constant} \tag{50}$$

$$\mathbf{\Phi}_{qi}^{roll} = \left[\; -\mathbf{a}_i^T, \; -\mathbf{a}_i^T \mathbf{B}_i \mathbf{s}_i^{'P} + \mathbf{a}_i^T \mathbf{R}^T \mathbf{d}_{ij} + \rho \; \right] / L \qquad \mathbf{\Phi}_{qj}^{roll} = \left[\; \mathbf{a}_i^T, \; \mathbf{a}_i^T \mathbf{B}_j \mathbf{s}_j^{'P} - \rho \; \right] / L \tag{51}$$

$$\nu^{\text{roll}} = 0 \qquad \gamma^{\text{roll}} = \gamma^{\text{pp2dd}} \qquad \eta^{\text{roll}} = \eta^{\text{pp2dd}} \qquad \sigma^{\text{roll}} = \sigma^{\text{pp2dd}} \tag{52}$$

The planar relative distance driver shown in (53–55) is based on the planar double-revolute constraint but uses distance as a function of time. It is much more difficult to add pure rolling to this constraint in that it uses the square of driver distance. Driver distance should never be negative.

$$\Phi^{\text{prdd}} = \mathbf{d}_{ij}^T \mathbf{d}_{ij} - \left(f(t) \right)^2 = 0 \qquad f(t) > 0 \tag{53}$$

$$\mathbf{\Phi}_{\text{qi}}^{\text{prdd}} = \mathbf{\Phi}_{\text{qi}}^{\text{rr}} \qquad \mathbf{\Phi}_{\text{qj}}^{\text{prdd}} = \mathbf{\Phi}_{\text{qj}}^{\text{rr}} \tag{54}$$

$$\begin{aligned} \nu^{\text{prdd}} &= 2 \; \mathrm{f} \; \mathrm{f_t} \qquad \gamma^{\text{prdd}} = \gamma^{\text{rr}} + 2 \; \mathrm{f_t}^2 + 2 \; \mathrm{f} \; \mathrm{f_{tt}} \\ \eta^{\text{prdd}} &= \eta^{\text{rr}} + 6 \; \mathrm{f_t} \; \mathrm{f_{tt}} + 2 \; \mathrm{f} \; \mathrm{f_{ttt}} \qquad \sigma^{\text{prdd}} = \sigma^{\text{rr}} + 6 \; \mathrm{f_{tt}}^2 + 8 \; \mathrm{f_t} \; \mathrm{f_{ttt}} + 2 \; \mathrm{f} \; \mathrm{f_{tttt}} \end{aligned} \tag{55}$$

4. Planar validation

Explicit geometric solutions for position, velocity, acceleration, jerk and jounce of four-bar and inverted slider-crank mechanisms shown in Fig. 1 were used for planar validation. The geometric solutions were validated using complex number loop equations.

Three kinematically driven numerical simulations were used to validate planar jerk and jounce constraints reported above. Input driver constraints were sinusoidal functions of time to provide non-zero driver jerk and jounce. The first planar numerical simulation was a four-bar mechanism with links 2 and 4 pinned to ground by revolute joints at points A and D and connected by a double-revolute constraint between points B and C (*nq=6, nc=5, nd=1*). Link 2 was driven by an absolute angle rotation driver θ as shown in (56) with $\theta_{START} = 30$ deg and $\theta_{DELTA} = 60$ deg. Output ψ was the angle of link 4. The second planar numerical simulation was an inverted slider-crank with links 2 and 4 pinned to ground by revolute joints at points E and F, a prismatic joint between link 2 and slider block 3, and a revolute joint at G between links 3 and 4 (*nq=9, nk=8, nd=1*). Planar parallel-1 and parallel-2 constraints were used to model the prismatic joint. Slider block 3 was driven by a planar parallel-2 distance driver and output ψ was the angle of link 4. The third numerical simulation was the same as the second but used a planar relative distance driver for the slider block.

$$\theta = \theta_{START} + \theta_{DELTA} \sin(2\pi \; t / \tau) \qquad \tau = 2 \text{ sec} \qquad h = \Delta t = 0.01 \text{ sec} \tag{56}$$

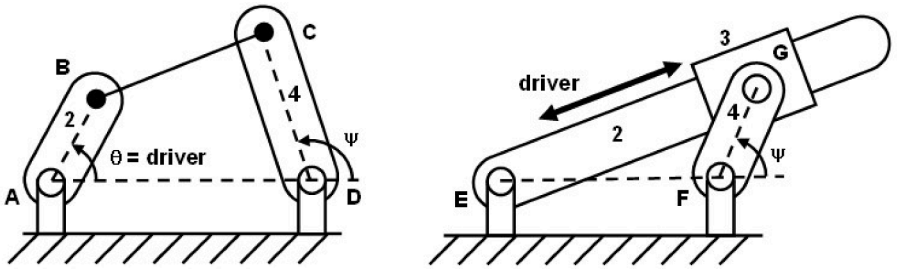

Fig. 1. – Four-bar (left) and inverted slider-crank (right) planar mechanisms (AD = 13.21 cm, AB = 4.00 cm, BC = 14.23 cm, CD = 20.31 cm, EF = 7.00 cm, FG = 2.00 cm, ψ = output).

Nominal assembly tolerance of 1e-12 was used to terminate iterative Newton-Raphson position solutions. All calculations were performed using MATLAB version R2019b [50].

Root-mean-square error (RMSE) between jerk simulations and geometric solutions for angular jerk of the output link of the planar four-bar mechanism was 1.07e-13 rad/sec^3 over one full cycle of the driver as shown in Fig. 2. RMSE for jounce was 9.7e-13 rad/sec^4 as shown in Fig. 3.

To assess the influence of assembly tolerance, the simulations were repeated for assembly tolerance ranging from 1e-14 to 1e-4. RMSE for planar velocity, RMSE for planar acceleration, RMSE for planar jerk and RMSE for planar jounce were normalized by their respective maximum absolute values and are shown as functions of assembly tolerance in Fig. 4. Normalized errors for planar jerk and jounce were effectively equal to normalized errors for planar velocity and acceleration. Normalized errors were at the computational accuracy floor of 1e-15 for assembly tolerance smaller than 1e-11.

Historically, computation of jerk and jounce required using first derivative and second derivative finite difference (FD) approximations applied to acceleration simulations. The second order central difference approximations shown in (57) and the fourth order central difference approximations provided in (58) from Fornberg [51] were applied to acceleration simulations to estimate FD jerk and jounce. Normalized RMSE between these FD approximations and geometric solutions are shown as functions of simulation time step in Fig. 5 for nominal assembly tolerance of 1e-12. Normalized RMSE for planar jerk and jounce from new equations presented above are also shown in Fig. 5.

$$\dot{u}_k \approx (-u_{k-1}+u_{k+1})\Big/2h \qquad \ddot{u}_k \approx (u_{k-1}-2u_k+u_{k+1})\Big/h^2 \tag{57}$$

$$\begin{aligned}\dot{u}_k &\approx (u_{k-2}-8u_{k-1}-8u_{k+1}-u_{k+2})/12h \\ \ddot{u}_k &\approx (-u_{k-2}+16u_{k-1}-30u_k+16u_{k+1}-u_{k+2})\Big/12h^2\end{aligned} \tag{58}$$

Normalized errors for new planar jerk and jounce equations developed for this paper are independent of simulation time step as expected and are significantly better than FD approximations.

Results from inverted slider-crank simulations are provided in Figs. 6 and 7 and are very similar to corresponding four-bar graphs.

5. Spatial kinematics

Spatial position, velocity and acceleration kinematics in (59–62) follow Haug [41]. The skew-symmetric operator shown in (60) is equivalent to a cross-product. Jerk (63–64) and jounce (65–66) were developed for this paper by taking time derivatives of acceleration (62). Relative position, velocity, acceleration and jerk vectors used to form planar constraints are provided in (67–72).

$$\mathbf{r}_i^{\mathbf{P}} = \mathbf{r}_i + \mathbf{A}_i \mathbf{s}_i^{\prime\mathbf{P}} \tag{59}$$

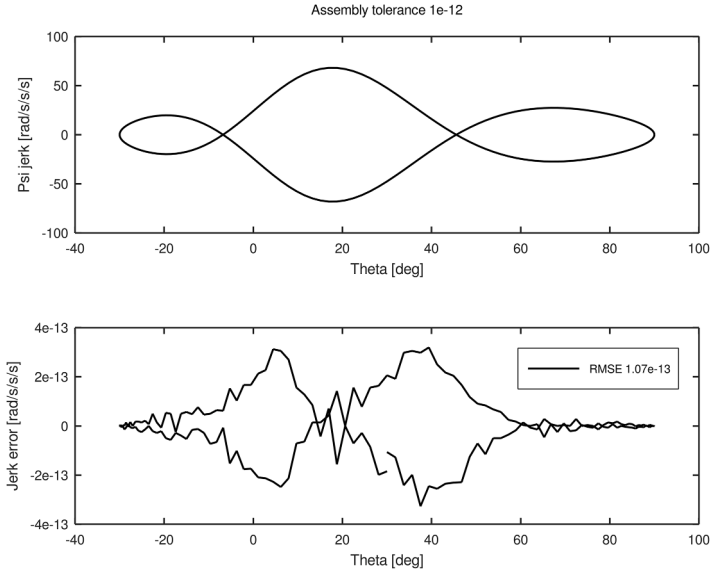

Fig. 2. – Jerk simulation for planar four-bar mechanism (top) and error between jerk simulation and geometric validation solution (bottom) using nominal assembly tolerance of 1e-12.

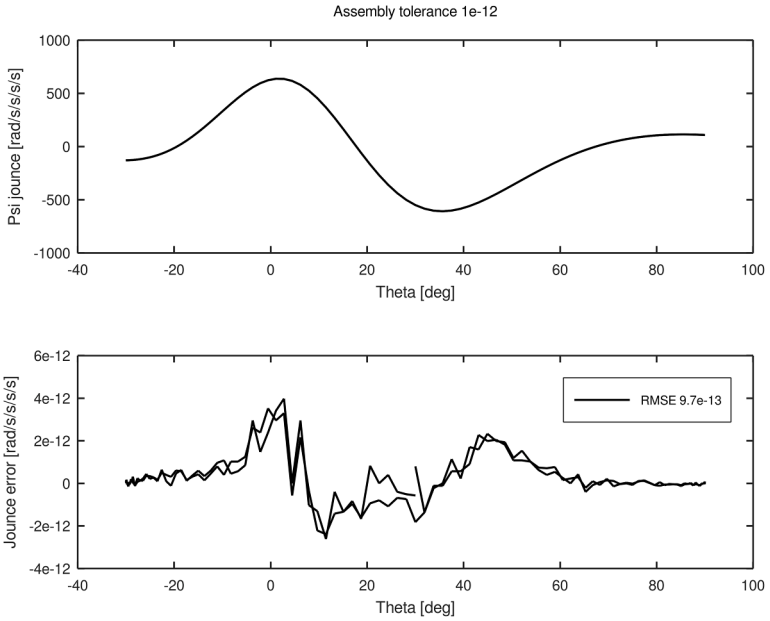

Fig. 3. – Jounce simulation for planar four-bar mechanism (top) and error between jounce simulation and geometric validation solution (bottom) using nominal assembly tolerance of 1e-12.

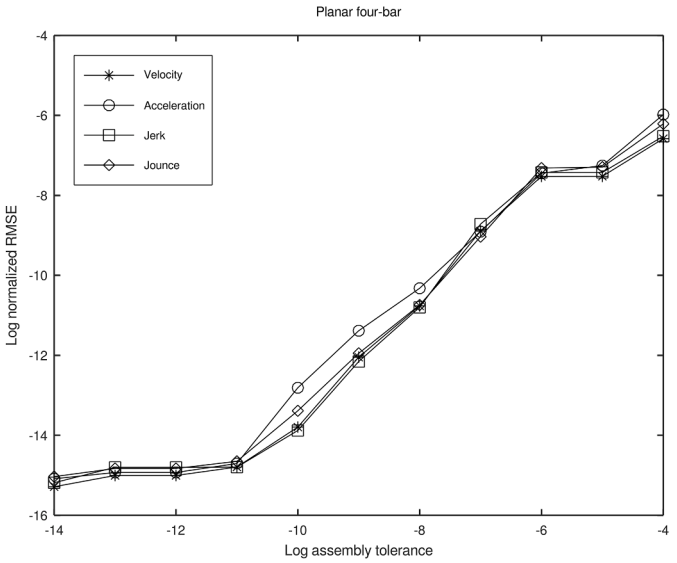

Fig. 4. – Relationship between assembly tolerance and RMSE for velocity, acceleration, jerk and jounce simulations of planar four-bar mechanism.

$$for \quad \boldsymbol{\omega_i}' = \begin{Bmatrix} \omega_{i\,x}' \\ \omega_{i\,y}' \\ \omega_{i\,z}' \end{Bmatrix}_{3x1} \quad then \quad \widetilde{\boldsymbol{\omega}}_{\mathbf{i}}' = \begin{bmatrix} 0 & -\omega_{i\,z}' & \omega_{i\,y}' \\ \omega_{i\,z}' & 0 & -\omega_{i\,x}' \\ -\omega_{i\,y}' & \omega_{i\,x}' & 0 \end{bmatrix}_{3x3} \tag{60}$$

$$\dot{\mathbf{r}}_{\mathbf{i}}^{\mathbf{P}} = \dot{\mathbf{r}}_{\mathbf{i}} + \mathbf{A}_{\mathbf{i}}\widetilde{\boldsymbol{\omega}}_{\mathbf{i}}'\mathbf{s}_{\mathbf{i}}^{\mathbf{P}} \tag{61}$$

$$\ddot{\mathbf{r}}_{\mathbf{i}}^{\mathbf{P}} = \ddot{\mathbf{r}}_{\mathbf{i}} + \mathbf{A}_{\mathbf{i}}\dot{\widetilde{\boldsymbol{\omega}}}_{\mathbf{i}}'\mathbf{s}_{\mathbf{i}}^{\mathbf{P}} + \mathbf{A}_{\mathbf{i}}\widetilde{\boldsymbol{\omega}}_{\mathbf{i}}'\widetilde{\boldsymbol{\omega}}_{\mathbf{i}}'\mathbf{s}_{\mathbf{i}}^{\mathbf{P}} \tag{62}$$

$$\mathbf{H}_{\mathbf{i}}' = 2\widetilde{\boldsymbol{\omega}}_{\mathbf{i}}'\dot{\widetilde{\boldsymbol{\omega}}}_{\mathbf{i}}' + \dot{\widetilde{\boldsymbol{\omega}}}_{\mathbf{i}}'\widetilde{\boldsymbol{\omega}}_{\mathbf{i}}' + \widetilde{\boldsymbol{\omega}}_{\mathbf{i}}'\widetilde{\boldsymbol{\omega}}_{\mathbf{i}}'\widetilde{\boldsymbol{\omega}}_{\mathbf{i}}' \tag{63}$$

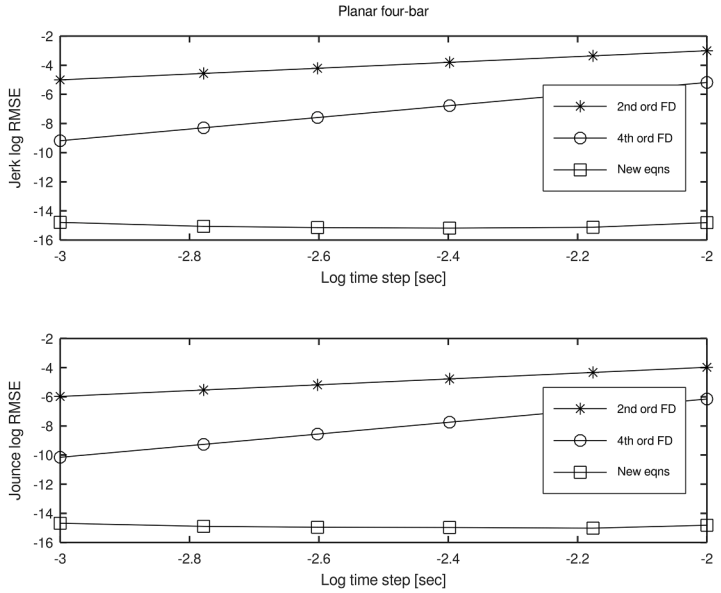

Fig. 5. – Relationship between simulation time step and normalized root-mean-square error (RMSE) for new planar jerk equations (top) and new planar jounce equations (bottom) compared to second and fourth order finite difference (FD) derivatives for planar four-bar simulations.

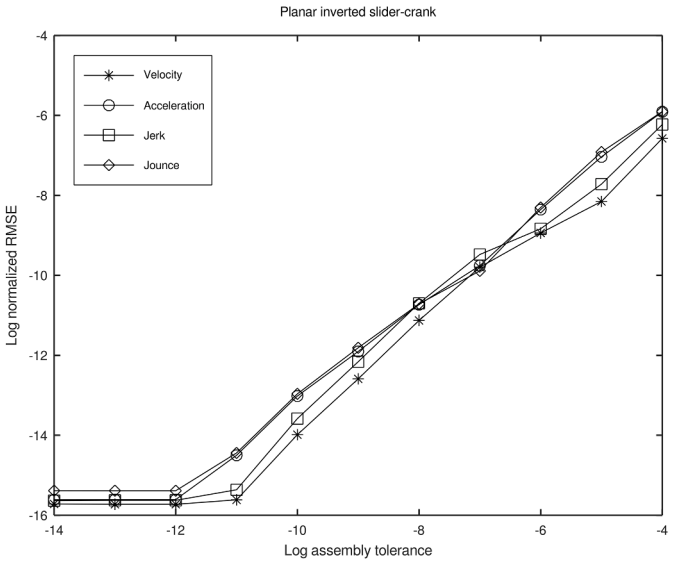

Fig. 6. – Relationship between assembly tolerance and RMSE for velocity, acceleration, jerk and jounce simulations of planar inverted slider-crank mechanism.

$$\dddot{\mathbf{r}}_i^{\mathbf{P}} = \dddot{\mathbf{r}}_i + \mathbf{A}_i\left(\mathbf{H}_i' + \ddot{\tilde{\omega}}_i'\right)\mathbf{s}_i'^{\mathbf{P}} \tag{64}$$

$$\mathbf{W}_i' = \dddot{\tilde{\omega}}_i'\tilde{\omega}_i' + 3\ddot{\tilde{\omega}}_i'\dot{\tilde{\omega}}_i' + 3\tilde{\omega}_i'\ddot{\tilde{\omega}}_i' + \dot{\tilde{\omega}}_i'\tilde{\omega}_i'\tilde{\omega}_i' + 2\tilde{\omega}_i'\dot{\tilde{\omega}}_i'\tilde{\omega}_i' + 3\tilde{\omega}_i'\tilde{\omega}_i'\dot{\tilde{\omega}}_i' + \tilde{\omega}_i'\tilde{\omega}_i'\tilde{\omega}_i'\tilde{\omega}_i' \tag{65}$$

$$\ddot{\mathbf{r}}_i^{\mathbf{P}} = \ddot{\mathbf{r}}_i + \mathbf{A}_i\left(\mathbf{W}_i' + \tilde{\omega}_i'\right)\mathbf{s}_i'^{\mathbf{P}} \tag{66}$$

$$\mathbf{d}_{ij} = \mathbf{r}_j^{\mathbf{P}} - \mathbf{r}_i^{\mathbf{P}} = \mathbf{r}_j + \mathbf{A}_j\mathbf{s}_j'^{\mathbf{P}} - \mathbf{r}_i - \mathbf{A}_i\mathbf{s}_i'^{\mathbf{P}} \tag{67}$$

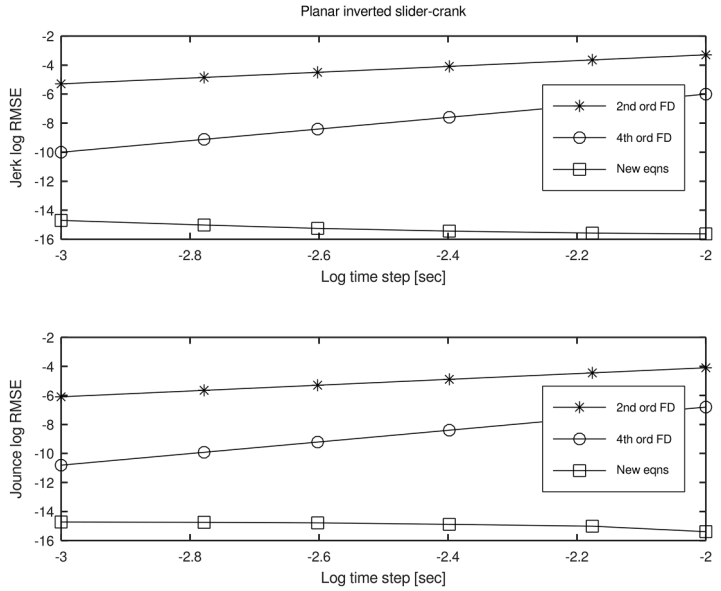

Fig. 7. – Relationship between simulation time step and normalized root-mean-square error (RMSE) for new planar jerk equations (top) and new planar jounce equations (bottom) compared to second and fourth order finite difference (FD) derivatives for planar inverted slider-crank simulations.

$$\dot{\mathbf{d}}_{ij} = \dot{\mathbf{r}}_j^P - \dot{\mathbf{r}}_i^P = \dot{\mathbf{r}}_j + \mathbf{A}_j\tilde{\boldsymbol{\omega}}_j'\mathbf{s}_j'^P - \dot{\mathbf{r}}_i - \mathbf{A}_i\tilde{\boldsymbol{\omega}}_i'\mathbf{s}_i'^P \tag{68}$$

$$\ddot{\mathbf{d}}_{ij} = \ddot{\mathbf{r}}_j^P - \ddot{\mathbf{r}}_i^P = \ddot{\mathbf{r}}_j + \mathbf{A}_j\tilde{\boldsymbol{\omega}}_j'\tilde{\boldsymbol{\omega}}_j'\mathbf{s}_j'^P + \mathbf{A}_j\dot{\tilde{\boldsymbol{\omega}}}_j'\mathbf{s}_j'^P - \ddot{\mathbf{r}}_i + \mathbf{A}_i\tilde{\boldsymbol{\omega}}_i'\tilde{\boldsymbol{\omega}}_i'\mathbf{s}_i'^P + \mathbf{A}_i\dot{\tilde{\boldsymbol{\omega}}}_i'\mathbf{s}_i'^P \tag{69}$$

$$\dddot{\mathbf{d}}_{ij} = \dddot{\mathbf{r}}_j^P - \dddot{\mathbf{r}}_i^P = \dddot{\mathbf{r}}_j + \mathbf{A}_j\left(\mathbf{H}_j' + \ddot{\tilde{\boldsymbol{\omega}}}_j'\right)\mathbf{s}_j'^P - \dddot{\mathbf{r}}_i - \mathbf{A}_i\left(\mathbf{H}_i' + \ddot{\tilde{\boldsymbol{\omega}}}_i'\right)\mathbf{s}_i'^P \tag{70}$$

$$\mathbf{a}_i = \mathbf{r}_i^Q - \mathbf{r}_i^P = \mathbf{A}_i\mathbf{a}_i' \tag{71}$$

$$\mathbf{a}_i' = \mathbf{s}_i'^Q - \mathbf{s}_i'^P \tag{72}$$

Transformations for angular velocity and angular acceleration between global and local body-fixed directions are provided in (73–74). Interestingly, transformations for angular jerk and angular jounce in (75–76) require additional terms.

$$\boldsymbol{\omega}_i = \mathbf{A}_i\boldsymbol{\omega}_i' \qquad \boldsymbol{\omega}_i' = \mathbf{A}_i^T\boldsymbol{\omega}_i \tag{73}$$

$$\dot{\boldsymbol{\omega}}_i = \mathbf{A}_i\dot{\boldsymbol{\omega}}_i' \qquad \dot{\boldsymbol{\omega}}_i' = \mathbf{A}_i^T\dot{\boldsymbol{\omega}}_i \tag{74}$$

$$\ddot{\boldsymbol{\omega}}_i = \mathbf{A}_i\left(\ddot{\boldsymbol{\omega}}_i' + \tilde{\boldsymbol{\omega}}_i'\dot{\boldsymbol{\omega}}_i'\right) \qquad \ddot{\boldsymbol{\omega}}_i' = \mathbf{A}_i^T\left(\ddot{\boldsymbol{\omega}}_i - \tilde{\boldsymbol{\omega}}_i\dot{\boldsymbol{\omega}}_i\right) \tag{75}$$

$$\dddot{\boldsymbol{\omega}}_i = \mathbf{A}_i\left(\dddot{\boldsymbol{\omega}}_i' + 2\tilde{\boldsymbol{\omega}}_i'\ddot{\boldsymbol{\omega}}_i' + (\dot{\tilde{\boldsymbol{\omega}}}_i' + \tilde{\boldsymbol{\omega}}_i'\tilde{\boldsymbol{\omega}}_i')\dot{\boldsymbol{\omega}}_i'\right) \qquad \dddot{\boldsymbol{\omega}}_i' = \mathbf{A}_i^T\left(\dddot{\boldsymbol{\omega}}_i - 2\tilde{\boldsymbol{\omega}}_i\ddot{\boldsymbol{\omega}}_i - (\dot{\tilde{\boldsymbol{\omega}}}_i - \tilde{\boldsymbol{\omega}}_i\tilde{\boldsymbol{\omega}}_i)\dot{\boldsymbol{\omega}}_i\right) \tag{76}$$

Spatial mechanical joints are modelled using four basic constraints provided below (spherical, double-spherical, spatial dot-1 and spatial dot-2) as described by Haug section 9.4.4 [41]. A spherical joint restricts three DOF and a double-spherical joint only restricts one DOF as shown below. A universal joint restricts four DOF and is modelled using a spherical constraint and one dot-1 constraint. A spatial revolute joint restricts five DOF and is modelled using a spherical constraint, one dot-1 constraint and one dot-2 constraint. A cylindrical joint restricts four DOF and is modelled using two dot-1 constraints and two dot-2 constraints. A spatial prismatic joint restricts five DOF and is modelled using three dot-1 constraints and two dot-2 constraints. Lastly a mechanical screw joint restricts five DOF and is modelled using two dot-1 constraints, two dot-2 constraints and a distance driver with f(t)=0.

Spherical joint constraints are shown in (77–80) following Haug [41]. Jerk RHS and jounce RHS were developed for this paper as

shown in (81–82). Derivations are provided in Appendix A.

$$\mathbf{\Phi}^{s} = \mathbf{d}_{ij} = \mathbf{r}_j^P - \mathbf{r}_i^P = \mathbf{0} \tag{77}$$

$$\mathbf{\Phi}^{s}_{ri} = -\mathbf{I}_3 \qquad \mathbf{\Phi}^{s}_{rj} = \mathbf{I}_3 \tag{78}$$

$$\mathbf{\Phi}^{s}_{\pi i'} = \mathbf{A}_i \widetilde{\mathbf{s}}_i'^{P} \qquad \mathbf{\Phi}^{s}_{\pi j'} = -\mathbf{A}_j \widetilde{\mathbf{s}}_j'^{P} \tag{79}$$

$$\boldsymbol{\gamma}^{s} = \mathbf{A}_i \widetilde{\boldsymbol{\omega}}_i' \widetilde{\boldsymbol{\omega}}_i' \mathbf{s}_i'^{P} - \mathbf{A}_j \widetilde{\boldsymbol{\omega}}_j' \widetilde{\boldsymbol{\omega}}_j' \mathbf{s}_j'^{P} \tag{80}$$

$$\boldsymbol{\eta}^{s} = \mathbf{A}_i \mathbf{H}_i' \mathbf{s}_i'^{P} - \mathbf{A}_j \mathbf{H}_j' \mathbf{s}_j'^{P} \tag{81}$$

$$\boldsymbol{\sigma}^{s} = \mathbf{A}_i \mathbf{W}_i' \mathbf{s}_i'^{P} - \mathbf{A}_j \mathbf{W}_j' \mathbf{s}_j'^{P} \tag{82}$$

Spatial double-spherical joint constraints are provided in (83–88). Note that Jacobian, acceleration RHS, jerk RHS and jounce RHS terms utilize corresponding terms from the spatial spherical for simplification.

$$\Phi^{ss} = \mathbf{d}_{ij}^T \mathbf{d}_{ij} - L^2 = \left(\mathbf{r}_j^P - \mathbf{r}_i^P\right)^T \left(\mathbf{r}_j^P - \mathbf{r}_i^P\right) - L^2 = 0 \qquad \text{L} = \text{constant length} \tag{83}$$

$$\mathbf{\Phi}^{ss}_{ri} = -2\mathbf{d}_{ij}^T \qquad \mathbf{\Phi}^{ss}_{rj} = 2\mathbf{d}_{ij}^T \tag{84}$$

$$\Phi^{ss}_{\pi i'} = 2\mathbf{d}_{ij}^T \mathbf{A}_i \widetilde{\mathbf{s}}_i'^{P} = 2\mathbf{d}_{ij}^T \mathbf{\Phi}^{s}_{\pi i'} \qquad \Phi^{ss}_{\pi j'} = -2\mathbf{d}_{ij}^T \mathbf{A}_j \widetilde{\mathbf{s}}_j'^{P} = 2\mathbf{d}_{ij}^T \mathbf{\Phi}^{s}_{\pi j'} \tag{85}$$

$$\gamma^{ss} = -2\dot{\mathbf{d}}_{ij}^T \dot{\mathbf{d}}_{ij} + 2\mathbf{d}_{ij}^T \boldsymbol{\gamma}^{s} \tag{86}$$

$$\eta^{ss} = -6\dot{\mathbf{d}}_{ij}^T \ddot{\mathbf{d}}_{ij} + 2\mathbf{d}_{ij}^T \boldsymbol{\eta}^{s} \tag{87}$$

$$\sigma^{ss} = -\mathbf{6}\ddot{\mathbf{d}}_{ij}^T \ddot{\mathbf{d}}_{ij} - 8\dot{\mathbf{d}}_{ij}^T \dddot{\mathbf{d}}_{ij} + \mathbf{2}\mathbf{d}_{ij}^T \boldsymbol{\sigma}^{s} \tag{88}$$

Spatial dot-1 constraints in (89–92) correct minor typographical errors for acceleration in Haug section 9.6.3 [41]. Jerk RHS and jounce RHS in (93–94) were developed for this paper.

$$\Phi^{d1} = \mathbf{a}_i^T \mathbf{a}_j = 0 \tag{89}$$

$$\mathbf{\Phi}^{d1}_{ri} = [0, 0, 0] \qquad \mathbf{\Phi}^{d1}_{rj} = [0, 0, 0] \tag{90}$$

$$\Phi^{d1}_{\pi i'} = -\mathbf{a}_j'^T \mathbf{A}_j^T \mathbf{A}_i \widetilde{\mathbf{a}}_i \qquad \Phi^{d1}_{\pi j'} = -\mathbf{a}_i'^T \mathbf{A}_i^T \mathbf{A}_j \widetilde{\mathbf{a}}_j \tag{91}$$

$$\boldsymbol{\gamma}^{d1} = -\mathbf{a}_j'^T \left(\mathbf{A}_j^T \mathbf{A}_i \widetilde{\boldsymbol{\omega}}_i' \widetilde{\boldsymbol{\omega}}_i' + \mathbf{2}\widetilde{\boldsymbol{\omega}}_j'^T \mathbf{A}_j^T \mathbf{A}_i \widetilde{\boldsymbol{\omega}}_i' + \widetilde{\boldsymbol{\omega}}_j' \widetilde{\boldsymbol{\omega}}_j' \mathbf{A}_j^T \mathbf{A}_i\right) \mathbf{a}_i' \tag{92}$$

$$\boldsymbol{\eta}^{d1} = -\mathbf{a}_j'^T \mathbf{A}_j^T \mathbf{A}_i \mathbf{H}_i' \mathbf{a}_i' - \mathbf{a}_i'^T \mathbf{A}_i^T \mathbf{A}_j \mathbf{H}_j' \mathbf{a}_j' - \mathbf{3}\mathbf{a}_j'^T (\widetilde{\boldsymbol{\omega}}_j' \widetilde{\boldsymbol{\omega}}_j' - \dot{\widetilde{\boldsymbol{\omega}}}_j') \mathbf{A}_j^T \mathbf{A}_i \widetilde{\boldsymbol{\omega}}_i' \mathbf{a}_i' - \mathbf{3}\mathbf{a}_i'^T (\widetilde{\boldsymbol{\omega}}_i' \widetilde{\boldsymbol{\omega}}_i' - \dot{\widetilde{\boldsymbol{\omega}}}_i') \mathbf{A}_i^T \mathbf{A}_j \widetilde{\boldsymbol{\omega}}_j' \mathbf{a}_j' \tag{93}$$

$$\begin{aligned} \boldsymbol{\sigma}^{d1} = & -\mathbf{a}_j'^T \mathbf{A}_j^T \mathbf{A}_i \mathbf{W}_i' \mathbf{a}_i' - \mathbf{a}_i'^T \mathbf{A}_i^T \mathbf{A}_j \mathbf{W}_j' \mathbf{a}_j' + \mathbf{4}\mathbf{a}_j'^T \widetilde{\boldsymbol{\omega}}_j' \mathbf{A}_j^T \mathbf{A}_i \left(\mathbf{H}_i' + \ddot{\widetilde{\boldsymbol{\omega}}}_i'\right) \mathbf{a}_i' + \mathbf{4}\mathbf{a}_i'^T \widetilde{\boldsymbol{\omega}}_i' \mathbf{A}_i^T \mathbf{A}_j \left(\mathbf{H}_j' + \ddot{\widetilde{\boldsymbol{\omega}}}_j'\right) \mathbf{a}_j' \\ & -\mathbf{6}\mathbf{a}_j'^T (\widetilde{\boldsymbol{\omega}}_j' \widetilde{\boldsymbol{\omega}}_j' - \dot{\widetilde{\boldsymbol{\omega}}}_j') \mathbf{A}_j^T \mathbf{A}_i (\widetilde{\boldsymbol{\omega}}_i' \widetilde{\boldsymbol{\omega}}_i' + \dot{\widetilde{\boldsymbol{\omega}}}_i') \mathbf{a}_i' \end{aligned} \tag{94}$$

Spatial dot-2 constraints in (95–98) follow Haug [41] and provide point-on-line motion. Jerk RHS and jounce RHS are provided in (99–100). Jacobian, acceleration RHS, jerk RHS and jounce RHS terms utilize corresponding terms from the spatial spherical for simplification.

$$\Phi^{d2} = \mathbf{a}_i^T \mathbf{d}_{ij} = \mathbf{a}_i^T \left(\mathbf{r}_j^P - \mathbf{r}_i^P\right) = 0 \tag{95}$$

$$\mathbf{\Phi}^{d2}_{ri} = -\mathbf{a}_i'^T \mathbf{A}_i^T = -\mathbf{a}_i^T \qquad \mathbf{\Phi}^{d2}_{rj} = \mathbf{a}_i'^T \mathbf{A}_i^T = \mathbf{a}_i^T \tag{96}$$

$$\mathbf{\Phi}^{d2}_{\pi i'} = \mathbf{a}_i'^T \widetilde{\mathbf{s}}_i'^{P} - \mathbf{d}_{ij}^T \mathbf{A}_i \widetilde{\mathbf{a}}_i' \qquad \mathbf{\Phi}^{d2}_{\pi j'} = -\mathbf{a}_i'^T \mathbf{A}_i^T \mathbf{A}_j \widetilde{\mathbf{s}}_j'^{P} = -\mathbf{a}_i^T \mathbf{\Phi}^{s}_{\pi j'} \tag{97}$$

$$\boldsymbol{\gamma}^{\mathbf{d2}} = -2\dot{\mathbf{d}}_{\mathbf{ij}}{}^{\mathbf{T}}\mathbf{A}_{\mathbf{i}}\widetilde{\boldsymbol{\omega}}_{\mathbf{i}}{}'\mathbf{a}_{\mathbf{i}}{}' - \mathbf{d}_{\mathbf{ij}}{}^{\mathbf{T}}\mathbf{A}_{\mathbf{i}}\widetilde{\boldsymbol{\omega}}_{\mathbf{i}}{}'\widetilde{\boldsymbol{\omega}}_{\mathbf{i}}{}'\mathbf{a}_{\mathbf{i}}{}' + \mathbf{a}_{\mathbf{i}}{}'^{\mathbf{T}}\mathbf{A}_{\mathbf{i}}{}^{\mathbf{T}}\boldsymbol{\gamma}^{\mathbf{s}} \tag{98}$$

$$\boldsymbol{\eta}^{\mathbf{d2}} = -3\ddot{\mathbf{d}}_{\mathbf{ij}}{}^{\mathbf{T}}\mathbf{A}_{\mathbf{i}}\widetilde{\boldsymbol{\omega}}_{\mathbf{i}}{}'\mathbf{a}_{\mathbf{i}}{}' - 3\dot{\mathbf{d}}_{\mathbf{ij}}{}^{\mathbf{T}}\mathbf{A}_{\mathbf{i}}(\widetilde{\boldsymbol{\omega}}_{\mathbf{i}}{}'\widetilde{\boldsymbol{\omega}}_{\mathbf{i}}{}' + \dot{\widetilde{\boldsymbol{\omega}}}_{\mathbf{i}})\mathbf{a}_{\mathbf{i}}{}' - \mathbf{d}_{\mathbf{ij}}{}^{\mathbf{T}}\mathbf{A}_{\mathbf{i}}\mathbf{H}_{\mathbf{i}}{}'\mathbf{a}_{\mathbf{i}}{}' + \mathbf{a}_{\mathbf{i}}{}'^{\mathbf{T}}\mathbf{A}_{\mathbf{i}}{}^{\mathbf{T}}\boldsymbol{\eta}^{\mathbf{s}} \tag{99}$$

$$\sigma^{\mathrm{d2}} = -4\dddot{\mathbf{d}}_{\mathbf{ij}}{}^{\mathbf{T}}\mathbf{A}_{\mathbf{i}}\widetilde{\boldsymbol{\omega}}_{\mathbf{i}}{}'\mathbf{a}_{\mathbf{i}}{}' - 6\ddot{\mathbf{d}}_{\mathbf{ij}}{}^{\mathbf{T}}\mathbf{A}_{\mathbf{i}}(\widetilde{\boldsymbol{\omega}}_{\mathbf{i}}{}'\widetilde{\boldsymbol{\omega}}_{\mathbf{i}}{}' + \dot{\widetilde{\boldsymbol{\omega}}}_{\mathbf{i}}{}')\mathbf{a}_{\mathbf{i}}{}' - 4\dot{\mathbf{d}}_{\mathbf{ij}}{}^{\mathbf{T}}\mathbf{A}_{\mathbf{i}}\left(\ddot{\widetilde{\boldsymbol{\omega}}}_{\mathbf{i}}{}' + \mathbf{H}_{\mathbf{i}}{}'\right)\mathbf{a}_{\mathbf{i}}{}' - \mathbf{d}_{\mathbf{ij}}{}^{\mathbf{T}}\mathbf{A}_{\mathbf{i}}\mathbf{W}_{\mathbf{i}}{}'\mathbf{a}_{\mathbf{i}}{}' + \mathbf{a}_{\mathbf{i}}{}'^{\mathbf{T}}\mathbf{A}_{\mathbf{i}}{}^{\mathbf{T}}\boldsymbol{\sigma}^{\mathbf{s}} \tag{100}$$

The fixed revolute rotation driver for body i with driver angle θ about fixed unit vector $\hat{\mathbf{u}}$ and Euler parameter quaternion $\mathbf{p_i} = [\mathrm{p_{i0}},\ \mathrm{p_{i1}},\ \mathrm{p_{i2}},\ \mathrm{p_{i3}}]^{\mathbf{T}}$ is provided in (101–102). Corresponding velocity, acceleration, jerk and jounce terms are presented in (103).

$$\Phi^{\mathrm{frrd}} = \theta - f(t) = 0 \qquad \sin(\theta/2) = \sqrt{\mathrm{p_{i1}^2 + p_{i2}^2 + p_{i3}^2}} \qquad \cos(\theta/2) = \mathrm{p_{i0}} \tag{101}$$

$$\boldsymbol{\Phi}^{\mathbf{frrd}}_{\mathbf{ri}} = [0,\ 0,\ 0] \qquad \boldsymbol{\Phi}^{\mathbf{frrd}}_{\boldsymbol{\pi} i} = \hat{\mathbf{u}}^{\mathbf{T}} \tag{102}$$

$$\nu^{\mathrm{frrd}} = \mathrm{f_t} \qquad \gamma^{\mathrm{frrd}} = \mathrm{f_{tt}} \qquad \eta^{\mathrm{frrd}} = \mathrm{f_{ttt}} \qquad \sigma^{\mathrm{frrd}} = \mathrm{f_{tttt}} \tag{103}$$

The spatial relative distance driver shown in (104–106) is based on the double-spherical constraint. Velocity, acceleration, jerk and jounce terms are shown in (107). Again, driver distance should never be negative.

$$\Phi^{\mathrm{srdd}} = \mathbf{d}_{ij}{}^{T}\mathbf{d}_{ij} - (f(t))^2 = 0 \qquad f(t) > 0 \tag{104}$$

$$\boldsymbol{\Phi}^{\mathbf{srdd}}_{\mathbf{ri}} = \Phi^{\mathbf{ss}}_{\mathbf{ri}} \qquad \boldsymbol{\Phi}^{\mathbf{srdd}}_{\mathbf{rj}} = \Phi^{\mathbf{ss}}_{\mathbf{rj}} \tag{105}$$

$$\boldsymbol{\Phi}^{\mathbf{srdd}}_{\boldsymbol{\pi} i} = \Phi^{\mathbf{ss}}_{\boldsymbol{\pi} i} \qquad \boldsymbol{\Phi}^{\mathbf{srdd}}_{\boldsymbol{\pi} j} = \Phi^{\mathbf{ss}}_{\boldsymbol{\pi} j} \tag{106}$$

$$\begin{aligned} &\nu^{\mathrm{srdd}} = 2\ \mathrm{f}\ \mathrm{f_t} \qquad \gamma^{\mathrm{srdd}} = \gamma^{\mathrm{ss}} + 2\ \mathrm{f_t}^2 + 2\ \mathrm{f}\ \mathrm{f_{tt}} \\ &\eta^{\mathrm{srdd}} = \eta^{\mathrm{ss}} + 6\ \mathrm{f_t}\ \mathrm{f_{tt}} + 2\ \mathrm{f}\ \mathrm{f_{ttt}} \qquad \sigma^{\mathrm{srdd}} = \sigma^{\mathrm{ss}} + 6\ \mathrm{f_{tt}}^2 + 8\ \mathrm{f_t}\ \mathrm{f_{ttt}} + 2\ \mathrm{f}\ \mathrm{f_{tttt}} \end{aligned} \tag{107}$$

The spatial dot-2 distance driver shown in (108–111) is an extension of the dot-2 constraint.

$$\Phi^{\mathrm{d2dd}} = \mathbf{a}_i{}^{T}\mathbf{d}_{ij}/L - f(t) = 0 \qquad L = |\mathbf{a}_i| = \text{constant length} \tag{108}$$

$$\boldsymbol{\Phi}^{\mathbf{d2dd}}_{\mathbf{ri}} = \Phi^{\mathbf{d2}}_{\mathbf{ri}}\Big/L \qquad \boldsymbol{\Phi}^{\mathbf{d2dd}}_{\mathbf{rj}} = \Phi^{\mathbf{d2}}_{\mathbf{rj}}\Big/L \tag{109}$$

$$\boldsymbol{\Phi}^{\mathbf{d2dd}}_{\boldsymbol{\pi} i'} = \boldsymbol{\Phi}^{\mathbf{d2}}_{\boldsymbol{\pi} i'}\Big/L \qquad \boldsymbol{\Phi}^{\mathbf{d2dd}}_{\boldsymbol{\pi} j'} = \boldsymbol{\Phi}^{\mathbf{d2}}_{\boldsymbol{\pi} j'}\Big/L \tag{110}$$

$$\nu^{\mathrm{d2dd}} = \mathrm{f_t} \qquad \gamma^{\mathrm{d2dd}} = \gamma^{\mathrm{d2}}/\mathrm{L} + \mathrm{f_{tt}} \qquad \eta^{\mathrm{d2dd}} = \eta^{\mathrm{d2}}/\mathrm{L} + \mathrm{f_{ttt}} \qquad \sigma^{\mathrm{d2dd}} = \sigma^{\mathrm{d2}}/\mathrm{L} + \mathrm{f_{tttt}} \tag{111}$$

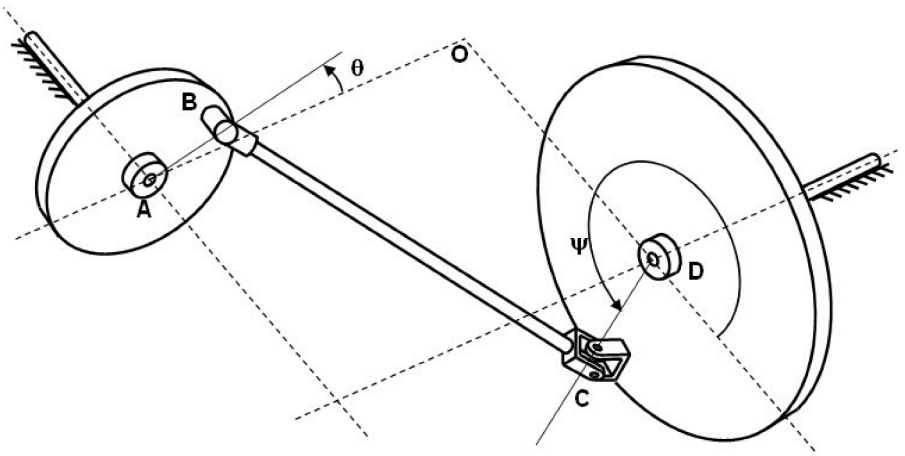

Fig. 8. – Revolute-spherical-universal-revolute (RSUR) spatial mechanism (OA = 20.43 cm, AB = 4.00 cm, CD = 10.00 cm, OD = 19.97 cm, BC = 30.42 cm, θ = input, ψ = output).

6. Spatial validation

Explicit geometric solutions for position, velocity, acceleration, jerk and jounce of the revolute-spherical-universal-revolute (RSUR) mechanism shown in Fig. 8 and the revolute-spherical-prismatic-universal (RSPU) mechanism shown in Fig. 9 were used for spatial validation. The geometric solutions were validated using Denavit-Hartenberg matrix loop methods reported by Sommer [38].

Four kinematically driven numerical simulations were developed to validate the spatial constraints reported above. Input driver constraints were sinusoidal functions of time similar to (56) to provide non-zero driver jerk and jounce. The first RSUR spatial numerical simulation used a spherical constraint and two dot-1 constraints for the revolute joint at point A, a spherical constraint at point B, a spherical and one dot-1 constraint for the universal joint at point C, and another spherical with two dot-1 constraints for the revolute joint at point D (*nq=18, nk=17, nd=1*). The revolute joint at A was driven by a fixed revolute rotation driver θ. Output was the angle ψ of link CD. The second spatial numerical simulation used only two rotating links connected to ground by revolute joints at points A and D. A double-spherical constraint was used to connect points B and C forming a revolute-spherical-spherical-revolute (RSSR) mechanism (*nq=12, nk=11, nd=1*). Again, the revolute joint at A was driven by a fixed revolute rotation driver. The third spatial numerical simulation was an RSPU mechanism that modelled the prismatic joint by two dot-1 constraints (spatial parallel-1), two dot-2 constraints (spatial parallel-2) and one additional dot-1 constraint (*nq=18, nk=17, nd=1*). The distance d between points B and D was driven by a spatial relative distance driver and the output was revolute angle θ. Lastly, the fourth spatial numerical simulation used the same RSPU mechanism but with a spatial dot-2 distance driver for distance d.

Nominal assembly tolerance of 1e-12 was used to terminate iterative Newton-Raphson position solutions. All calculations were performed using MATLAB version R2019b [50].

RMSE between jerk simulations and geometric solutions for angular jerk of the output link of the RSUR was 2.17e-14 rad/sec^3 over one full cycle of the driver and RMSE for jounce was 3.81e-13 rad/sec^4.

Again, RMSE for spatial velocity, RMSE for spatial acceleration, RMSE for spatial jerk and RMSE for spatial jounce were normalized by their respective maximum absolute values and are shown as functions of assembly tolerance in Fig. 10. Normalized errors for spatial jerk and jounce were effectively equal to normalized errors for spatial velocity and acceleration and were at the computational accuracy floor of 1e-15 for assembly tolerance smaller than 1e-12.

Similar results were observed for RSSR simulations.

Normalized RMSE between second and fourth order FD approximations for spatial jerk and jounce and corresponding geometric solutions are shown as functions of simulation time step in Fig. 11. Normalized RMSE for spatial jerk and jounce from new equations presented above are also shown in Fig. 11. Similarly to planar results, new spatial jerk and jounce equations are significantly more accurate than FD approximations and are independent of simulation time step.

Results from RSPU simulations are provided in Figs. 12 and 13 and are very similar to corresponding RSUR graphs.

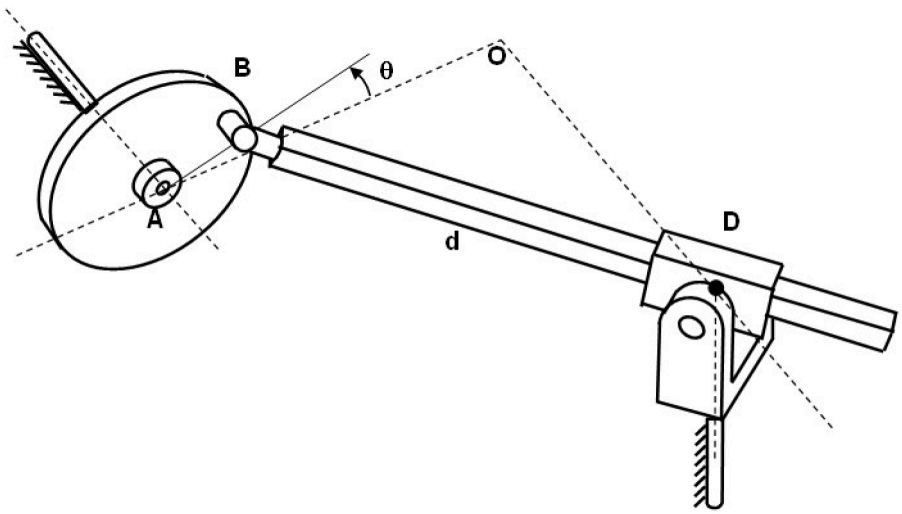

Fig. 9. – Revolute-spherical-prismatic-universal (RSPU) spatial mechanism (OA = 20.43 cm, AB = 4.00, OD = 19.97 cm, d = BD = input, θ = output).

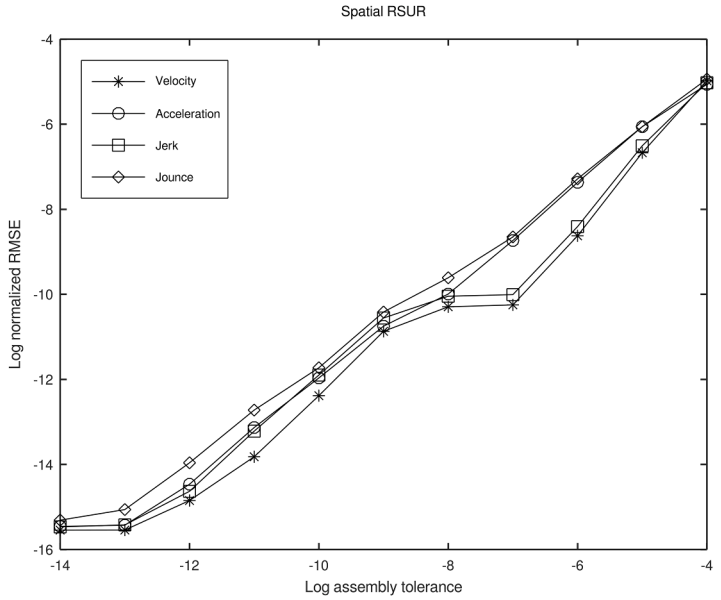

Fig. 10. – Relationship between assembly tolerance and RMSE for velocity, acceleration, jerk and jounce simulations of spatial RSUR mechanism.

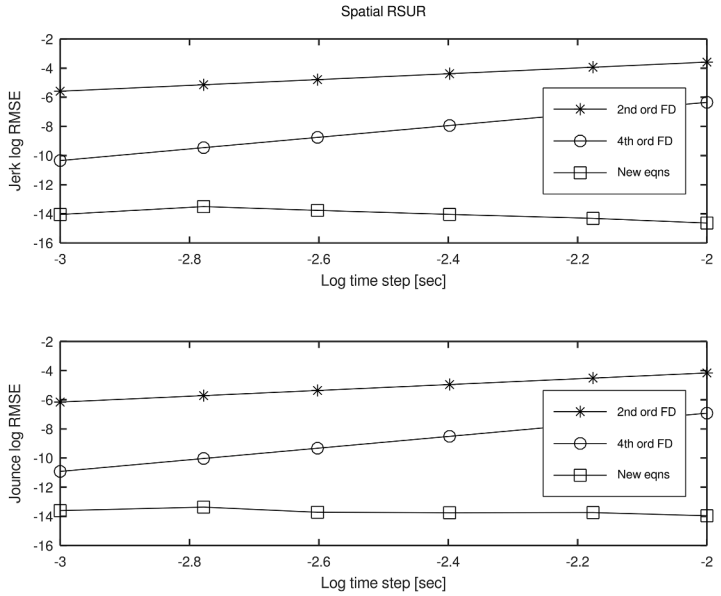

Fig. 11. – Relationship between simulation time step and normalized root-mean-square error (RMSE) for new spatial jerk equations (top) and new spatial jounce equations (bottom) compared to second and fourth order finite difference (FD) derivatives for spatial RSUR mechanism.

7. Conclusions

New equations for planar and spatial jerk and jounce were successfully validated against explicit geometric solutions. Kinematically driven simulations of planar four-bar and inverted slider-crank mechanisms as well as spatial RSUR and RSPU mechanisms tested these new equations.

It was very easy to modify extant velocity and acceleration simulation code because jerk and jounce solutions used the same Jacobian $\mathbf{\Phi_q}$. The only additional code required was to assemble jerk RHS $\boldsymbol{\eta}$ and jounce RHS $\boldsymbol{\sigma}$ vectors. This has two implications for implementing jerk and jounce into extant commercial simulation packages. First, execution time for commercial simulations will not be adversely affected because the inverse of the Jacobian is already available for velocity and acceleration solutions. This is particularly important for large scale spatial simulations with many moving bodies where the Jacobian can become very large with order 6 *nb* and inversion can be computationally expensive. Secondly, the additional computational burden to assemble jerk RHS $\boldsymbol{\eta}$ and jounce

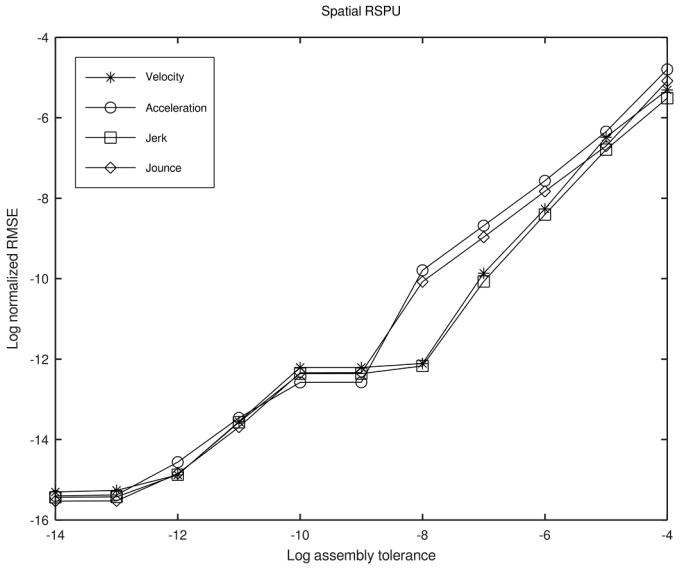

Fig. 12. – Relationship between assembly tolerance and RMSE for velocity, acceleration, jerk and jounce simulations of spatial RSPU mechanism.

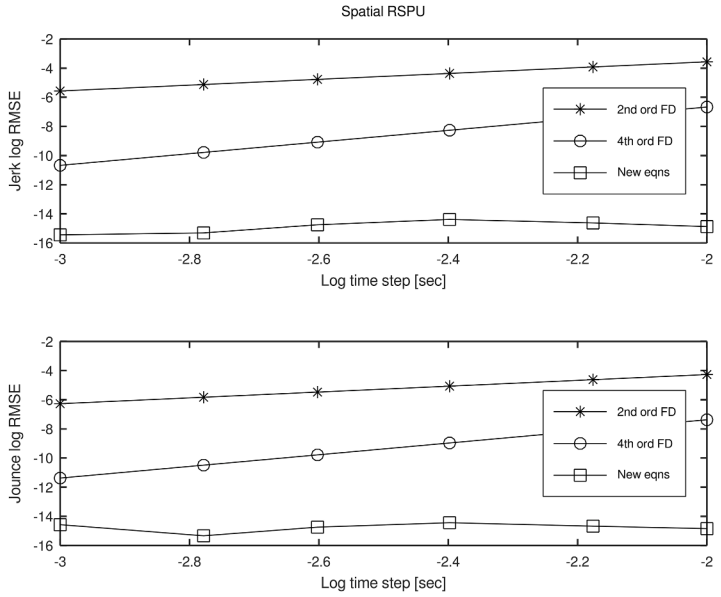

Fig. 13. – Relationship between simulation time step and normalized root-mean-square error (RMSE) for new planar jerk equations (top) and new planar jounce equations (bottom) compared to second and fourth order finite difference (FD) derivatives for spatial RSPU simulations.

RHS σ vectors is relatively small as demonstrated by Sommer [45] for forward dynamics of planar mechanisms.

Differences between kinematic simulations and explicit geometric solutions reported in Figs. 4, 6, 10 and 12 were directly related to assembly tolerance used to terminate iterative Newton-Raphson position solutions. Assembly tolerance of 1e-12 is recommended. This indicates that position residual error generated during forward time integration of multibody differential algebraic equations (DAE) must be smaller than 1e-12 for accurate results.

Relative precisions for new jerk and jounce computations are equivalent to relative precisions for velocity and acceleration computations. The new equations are significantly more accurate than second and fourth order FD approximations and are independent of simulation time step as shown in Figs. 5, 7, 11 and 13. These new equations completely preclude artifactual phase lag in real-time computations of jerk and jounce using backward difference FD approximations.

Planar jerk kinematics for revolute joints were used to develop hyper-dynamic third-order DAE for two planar rigid body mechanisms [45] using the first derivative of EOM. Hyper-dynamic DAE computed multibody jerk along with time derivatives of constraint reaction forces. That study showed that forward time integration of jerk simultaneously with acceleration using Obreshkov integrators

provided nominally ten times more accurate results compared to traditional simulations of EOM that only integrated acceleration. The implication is that incorporating jerk into commercial simulation packages could significantly increase integration accuracy or, conversely, decrease computation time for a given accuracy expectation.

Planar jerk equations developed for this paper allow simulation of first derivative of planar EOM to be expanded with more kinematic joints and drivers beyond only revolute joints. Spatial jerk equations developed for this paper now enable simulation of spatial hyper-dynamic DAE provided by Sommer [45] for future work. Planar and spatial jounce equations are now available to formulate second derivative of EOM using joint constraint kinematics as an alternative to screw mechanics [48–49].

CRediT authorship contribution statement

H.J. Sommer: Writing – review & editing, Writing – original draft, Visualization, Validation, Supervision, Software, Project administration, Methodology, Investigation, Formal analysis, Conceptualization.

Declaration of competing interest

The author declares that they have no known competing financial interests or personal relationships that could have appeared to influence the work reported in this paper.

Data availability

No data was used for the research described in the article.

Appendix A. – Derivations of jerk and jounce right-hand-side vectors

Derivations of jerk RHS $\boldsymbol{\eta}$ and jounce RHS $\boldsymbol{\sigma}$ for a planar revolute joint and for a spatial spherical joint are provided as exemplars of derivations for other joint and driver RHS vectors.

Jerk RHS $\boldsymbol{\eta}^{\mathbf{r}}$ for a planar revolute joint must conform to (7) as shown in (A1). Jacobian terms from (22) and acceleration RHS $\boldsymbol{\gamma}^{\mathbf{r}}$ from (23) and are reproduced in (A2-A3) for convenience. The first time derivative of the acceleration RHS is shown in (A4). Generalized accelerations for a revolute joint are shown in (A5) and their product with Jacobian terms is shown in (A6). Partial derivatives with respect to generalized coordinates are shown in (A7) and the final product with generalized velocities is provided in (A8). Substituting into (A1) provides jerk RHS $\boldsymbol{\eta}^{\mathbf{r}}$ in (A9) which matches (24).

$$\boldsymbol{\eta}^{\mathbf{r}} = \dot{\boldsymbol{\gamma}}^{\mathbf{r}} - \left(\boldsymbol{\Phi}^{\mathbf{r}}_{\mathbf{q}}\ddot{\mathbf{q}}\right)_{\mathbf{q}}\dot{\mathbf{q}} \tag{A1}$$

$$\boldsymbol{\Phi}^{r}_{qi} = \left[\ -\mathbf{I_2}\ ,\ -\mathbf{B}_i\mathbf{s}_i^{'P}\ \right] \qquad \boldsymbol{\Phi}^{r}_{qj} = \left[\ \mathbf{I_2}\ ,\ \mathbf{B}_j\mathbf{s}_j^{'P}\ \right] \tag{A2}$$

$$\boldsymbol{\gamma}^{\mathbf{r}} = \dot{\phi}_j^2\mathbf{A_j}\mathbf{s_j}^{'\mathbf{P}} - \dot{\phi}_i^2\mathbf{A}_i\mathbf{s}_i^{'P} \tag{A3}$$

$$\dot{\boldsymbol{\gamma}}^{r} = \dot{\phi}_j^3\mathbf{B_j}\mathbf{s_j}^{'\mathbf{P}} + 2\dot{\phi}_j\ddot{\phi}_j\mathbf{A_j}\mathbf{s_j}^{'\mathbf{P}} - \dot{\phi}_i^3\mathbf{B_i}\mathbf{s_i}^{'\mathbf{P}} - 2\dot{\phi}_i\ddot{\phi}_i\mathbf{A_i}\mathbf{s_i}^{'\mathbf{P}} \tag{A4}$$

$$\ddot{\mathbf{q}}_{\mathbf{i}} = \begin{Bmatrix} \ddot{\mathbf{r}}_{\mathbf{i}} \\ \ddot{\phi}_{\mathbf{i}} \end{Bmatrix} \qquad \ddot{\mathbf{q}}_j = \begin{Bmatrix} \ddot{\mathbf{r}}_{\mathbf{j}} \\ \ddot{\phi}_j \end{Bmatrix} \tag{A5}$$

$$\boldsymbol{\Phi}^{r}_{q}\ddot{\mathbf{q}} = -\ddot{\mathbf{r}}_{\mathbf{i}}\ -\ddot{\phi}_i\mathbf{B_i}\mathbf{s_i}^{'\mathbf{P}} + \ddot{\mathbf{r}}_{\mathbf{j}}\ +\ddot{\phi}_j\mathbf{B_j}\mathbf{s_j}^{'\mathbf{P}} \tag{A6}$$

$$\left(\boldsymbol{\Phi}^{\mathbf{r}}_{\mathbf{q}}\ddot{\mathbf{q}}\right)_{\mathbf{qi}} = \left[\mathbf{0_{2x2}},\ \ddot{\phi}_i\mathbf{A_i}\mathbf{s_i}^{'\mathbf{P}}\right] \qquad \left(\boldsymbol{\Phi}^{\mathbf{r}}_{\mathbf{q}}\ddot{\mathbf{q}}\right)_{\mathbf{qj}} = \left[\mathbf{0_{2x2}},\ -\ddot{\phi}_j\mathbf{A_j}\mathbf{s_j}^{'\mathbf{P}}\right] \tag{A7}$$

$$\left(\boldsymbol{\Phi}^{r}_{q}\ddot{\mathbf{q}}\right)_{q}\dot{\mathbf{q}} = \dot{\phi}_i\ddot{\phi}_i\mathbf{A}_i\mathbf{s}_i^{'P} - \dot{\phi}_j\ddot{\phi}_j\mathbf{A}_j\mathbf{s}_j^{'P} \tag{A8}$$

$$\boldsymbol{\eta}^{\mathbf{r}} = 3\dot{\phi}_j\ddot{\phi}_j\mathbf{A}_j\mathbf{s}_j^{'P} + \dot{\phi}_j^3\mathbf{B}_j\mathbf{s}_j^{'P} - 3\dot{\phi}_i\ddot{\phi}_i\mathbf{A}_i\mathbf{s}_i^{'P} - \dot{\phi}_i^3\mathbf{B}_i\mathbf{s}_i^{'P} \tag{A9}$$

Jounce RHS $\boldsymbol{\sigma}^{\mathbf{r}}$ for a revolute joint must conform to (8) as shown in (A10). The first time derivative of the jerk RHS is provided in (A11). Generalized jerks for a revolute joint are shown in (A12) and their product with Jacobian terms is shown in (A13). Partial derivatives with respect to generalized coordinates are shown in (A14) and the final product with generalized velocities is provided in (A15). Substituting into (A10) provides jounce RHS $\boldsymbol{\sigma}^{\mathbf{r}}$ in (A16) which matches (25).

$$\boldsymbol{\sigma}^{\mathbf{r}} = \dot{\boldsymbol{\eta}}^{\mathbf{r}} - \left(\boldsymbol{\Phi}^{\mathbf{r}}_{\mathbf{q}}\dddot{\mathbf{q}}\right)_{\mathbf{q}}\dot{\mathbf{q}} \tag{A10}$$

$$\dot{\eta}^{r} = -\dot{\phi}_j^4\mathbf{A}_j\mathbf{s}_j^{'P} + 6\dot{\phi}_j^2\ddot{\phi}_j\mathbf{B}_j\mathbf{s}_j^{'P} + 3\ddot{\phi}_j^2\mathbf{A}_j\mathbf{s}_j^{'P} + 3\dddot{\phi}_j\phi_j\mathbf{A}_j\mathbf{s}_j^{'P} + \dot{\phi}_i^4\mathbf{A}_i\mathbf{s}_i^{'P} - 6\dot{\phi}_i^2\ddot{\phi}_i\mathbf{B}_i\mathbf{s}_i^{'P} - 3\ddot{\phi}_i^2\mathbf{A}_i\mathbf{s}_i^{'P} - 3\dddot{\phi}_i\phi_i\mathbf{A}_i\mathbf{s}_i^{'P} \tag{A11}$$

$$\dddot{\mathbf{q}}_{\mathbf{i}} = \begin{Bmatrix} \dddot{\mathbf{r}}_{\mathbf{i}} \\ \dddot{\phi}_i \end{Bmatrix} \qquad \dddot{\mathbf{q}}_j = \begin{Bmatrix} \dddot{\mathbf{r}}_{\mathbf{j}} \\ \dddot{\phi}_j \end{Bmatrix} \tag{A12}$$

$$\boldsymbol{\Phi}^{r}_{q}\dddot{\mathbf{q}} = -\dddot{\mathbf{r}}_i - \dddot{\phi}_i\mathbf{B}_i\mathbf{s}_i^{'P} + \dddot{\mathbf{r}}_j + \dddot{\phi}_j\mathbf{B}_j\mathbf{s}_j^{'P} \tag{A13}$$

$$\left(\boldsymbol{\Phi}^{\mathbf{r}}_{\mathbf{q}}\dddot{\mathbf{q}}\right)_{\mathbf{qi}} = \left[\mathbf{0}_{\mathbf{2x2}},\ \dddot{\phi}_i\mathbf{A}_i\mathbf{s}_{\mathbf{i}}^{'\mathbf{P}}\right] \qquad \left(\boldsymbol{\Phi}^{\mathbf{r}}_{\mathbf{q}}\dddot{\mathbf{q}}\right)_{\mathbf{qj}} = \left[\mathbf{0}_{\mathbf{2x2}},\ -\dddot{\phi}_j\mathbf{A}_{\mathbf{j}}\mathbf{s}_{\mathbf{j}}^{'\mathbf{P}}\right] \tag{A14}$$

$$\left(\boldsymbol{\Phi}^{r}_{q}\dddot{\mathbf{q}}\right)_{q}\dot{\mathbf{q}} = \dddot{\phi}_i\mathbf{A}_i\mathbf{s}_i^{'P} - \dddot{\phi}_j\mathbf{A}_j\mathbf{s}_j^{'P} \tag{A15}$$

$$\boldsymbol{\sigma}^{r} = -\dot{\phi}_j^4\mathbf{A}_j\mathbf{s}_j^{'P} + 6\dot{\phi}_j^2\ddot{\phi}_j\mathbf{B}_j\mathbf{s}_j^{'P} + 3\ddot{\phi}_j^2\mathbf{A}_j\mathbf{s}_j^{'P} + 4\dddot{\phi}_j\phi_j\mathbf{A}_j\mathbf{s}_j^{'P} + \dot{\phi}_i^4\mathbf{A}_i\mathbf{s}_i^{'P} - 6\dot{\phi}_i^2\ddot{\phi}_i\mathbf{B}_i\mathbf{s}_i^{'P} - 3\ddot{\phi}_i^2\mathbf{A}_i\mathbf{s}_i^{'P} - 4\dddot{\phi}_i\phi_i\mathbf{A}_i\mathbf{s}_i^{'P} \tag{A16}$$

Jerk RHS $\boldsymbol{\eta}^{\mathbf{s}}$ for a spherical joint must conform to (7) as shown in (A17). Jacobian terms from (78–79) and acceleration RHS $\boldsymbol{\gamma}^{\mathbf{s}}$ from (80) and are reproduced in (A18-A20) for convenience. The first time derivative of the acceleration RHS is provided in (A21). Generalized accelerations for a spherical joint are shown in (A22) and their product with Jacobian terms is shown in (A23). Partial derivatives with respect to generalized coordinates are shown in (A24) and the final product with generalized velocities is provided in (A25). Substituting into (A17) provides jerk RHS $\boldsymbol{\eta}^{\mathbf{s}}$ in (A26) which matches (81).

$$\boldsymbol{\eta}^{\mathbf{s}} = \dot{\boldsymbol{\gamma}}^{s} - \left(\Phi^{\mathbf{s}}_{\mathbf{q}}\ddot{\mathbf{q}}\right)_{\mathbf{q}}\dot{\mathbf{q}} \tag{A17}$$

$$\boldsymbol{\Phi}^{\mathbf{s}}_{\mathbf{ri}} = -\mathbf{I}_3 \qquad \boldsymbol{\Phi}^{\mathbf{s}}_{\mathbf{rj}} = \mathbf{I}_3 \tag{A18}$$

$$\boldsymbol{\Phi}^{\mathbf{s}}_{\pi i'} = \mathbf{A}_{\mathbf{i}}\widetilde{\mathbf{s}}_{\mathbf{i}}^{'\mathbf{P}} \qquad \boldsymbol{\Phi}^{\mathbf{s}}_{\pi j'} = -\mathbf{A}_{\mathbf{j}}\widetilde{\mathbf{s}}_{\mathbf{j}}^{'\mathbf{P}} \tag{A19}$$

$$\boldsymbol{\gamma}^{\mathbf{s}} = \mathbf{A}_{\mathbf{i}}\widetilde{\boldsymbol{\omega}}_{\mathbf{i}}^{'}\widetilde{\boldsymbol{\omega}}_{\mathbf{i}}^{'}\mathbf{s}_{\mathbf{i}}^{'\mathbf{P}} - \mathbf{A}_{\mathbf{j}}\widetilde{\boldsymbol{\omega}}_{\mathbf{j}}^{'}\widetilde{\boldsymbol{\omega}}_{\mathbf{j}}^{'}\mathbf{s}_{\mathbf{j}}^{'\mathbf{P}} \tag{A20}$$

$$\dot{\boldsymbol{\gamma}}^{\mathbf{s}} = \mathbf{A}_{\mathbf{i}}(\widetilde{\boldsymbol{\omega}}_{\mathbf{i}}^{'}\widetilde{\boldsymbol{\omega}}_{\mathbf{i}}^{'}\widetilde{\boldsymbol{\omega}}_{\mathbf{i}}^{'} + \dot{\widetilde{\boldsymbol{\omega}}}_{\mathbf{i}}^{'}\widetilde{\boldsymbol{\omega}}_{\mathbf{i}}^{'} + \widetilde{\boldsymbol{\omega}}_{\mathbf{i}}^{'}\dot{\widetilde{\boldsymbol{\omega}}}_{\mathbf{i}}^{'})\mathbf{s}_{\mathbf{i}}^{'\mathbf{P}} - \mathbf{A}_{\mathbf{j}}(\widetilde{\boldsymbol{\omega}}_{\mathbf{j}}^{'}\widetilde{\boldsymbol{\omega}}_{\mathbf{j}}^{'}\widetilde{\boldsymbol{\omega}}_{\mathbf{j}}^{'} + \dot{\widetilde{\boldsymbol{\omega}}}_{\mathbf{j}}^{'}\widetilde{\boldsymbol{\omega}}_{\mathbf{j}}^{'} + \widetilde{\boldsymbol{\omega}}_{\mathbf{j}}^{'}\dot{\widetilde{\boldsymbol{\omega}}}_{\mathbf{j}}^{'})\mathbf{s}_{\mathbf{j}}^{'\mathbf{P}} \tag{A21}$$

$$\ddot{\mathbf{q}}_{\mathbf{i}} = \begin{Bmatrix} \ddot{\mathbf{r}}_{\mathbf{i}} \\ \dot{\omega}_{\mathbf{i}}^{'} \end{Bmatrix} \qquad \ddot{\mathbf{q}}_{\mathbf{j}} = \begin{Bmatrix} \ddot{\mathbf{r}}_{\mathbf{j}} \\ \dot{\omega}_{\mathbf{j}}^{'} \end{Bmatrix} \tag{A22}$$

$$\boldsymbol{\Phi}_{\mathbf{q}}\ddot{q} = -\ddot{\mathbf{r}}_{\mathbf{i}} - \mathbf{A}_{\mathbf{i}}\dot{\widetilde{\boldsymbol{\omega}}}_{\mathbf{i}}^{'}\mathbf{s}_{\mathbf{i}}^{'\mathbf{P}} + \ddot{\mathbf{r}}_{\mathbf{j}} + \mathbf{A}_{\mathbf{j}}\dot{\widetilde{\boldsymbol{\omega}}}_{\mathbf{j}}^{'}\mathbf{s}_{\mathbf{j}}^{'\mathbf{P}} \tag{A23}$$

$$\begin{aligned} \left(\Phi_{\mathbf{q}}\ddot{\mathbf{q}}\right)_{\mathbf{ri}} &= \mathbf{0}_{\mathbf{3x3}} \qquad \left(\Phi_{\mathbf{q}}\ddot{\mathbf{q}}\right)_{\pi i'} = \mathbf{A}_{\mathbf{i}}\left(\dot{\widetilde{\boldsymbol{\omega}}}_{\mathbf{i}}^{'}\widetilde{\mathbf{s}}_{\mathbf{i}}^{'\mathbf{P}} - \widetilde{\mathbf{s}}_{\mathbf{i}}^{'\mathbf{P}}\dot{\widetilde{\boldsymbol{\omega}}}_{\mathbf{i}}^{'}\right) \\ \left(\Phi_{\mathbf{q}}\ddot{\mathbf{q}}\right)_{\mathbf{rj}} &= \mathbf{0}_{\mathbf{3x3}} \qquad \left(\Phi_{\mathbf{q}}\ddot{\mathbf{q}}\right)_{\pi j'} = -\mathbf{A}_{\mathbf{j}}\left(\dot{\widetilde{\boldsymbol{\omega}}}_{\mathbf{j}}^{'}\widetilde{\mathbf{s}}_{\mathbf{j}}^{'\mathbf{P}} - \widetilde{\mathbf{s}}_{\mathbf{j}}^{'\mathbf{P}}\dot{\widetilde{\boldsymbol{\omega}}}_{\mathbf{j}}^{'}\right) \end{aligned} \tag{A24}$$

$$\left(\Phi_{\mathbf{q}}\ddot{\mathbf{q}}\right)_{\mathbf{q}}\dot{\mathbf{q}} = -\mathbf{A}_{\mathbf{i}}\widetilde{\boldsymbol{\omega}}_{\mathbf{i}}^{'}\dot{\widetilde{\boldsymbol{\omega}}}_{\mathbf{i}}^{'}\mathbf{s}_{\mathbf{i}}^{'\mathbf{P}} + \mathbf{A}_{\mathbf{j}}\widetilde{\boldsymbol{\omega}}_{\mathbf{j}}^{'}\dot{\widetilde{\boldsymbol{\omega}}}_{\mathbf{j}}^{'}\mathbf{s}_{\mathbf{j}}^{'\mathbf{P}} \tag{A25}$$

$$\boldsymbol{\eta}^{\mathbf{s}} = \mathbf{A}_{\mathbf{i}}(2\widetilde{\boldsymbol{\omega}}_{\mathbf{i}}^{'}\dot{\widetilde{\boldsymbol{\omega}}}_{\mathbf{i}}^{'} + \dot{\widetilde{\boldsymbol{\omega}}}_{\mathbf{i}}^{'}\widetilde{\boldsymbol{\omega}}_{\mathbf{i}}^{'} + \widetilde{\boldsymbol{\omega}}_{\mathbf{i}}^{'}\widetilde{\boldsymbol{\omega}}_{\mathbf{i}}^{'}\widetilde{\boldsymbol{\omega}}_{\mathbf{i}}^{'})\mathbf{s}_{\mathbf{i}}^{'\mathbf{P}} - \mathbf{A}_{\mathbf{j}}\left(2\widetilde{\boldsymbol{\omega}}_{\mathbf{j}}^{'}\dot{\widetilde{\boldsymbol{\omega}}}_{\mathbf{j}}^{'} + \dot{\widetilde{\boldsymbol{\omega}}}_{\mathbf{j}}^{'}\widetilde{\boldsymbol{\omega}}_{\mathbf{j}}^{'} + \widetilde{\boldsymbol{\omega}}_{\mathbf{j}}^{'}\widetilde{\boldsymbol{\omega}}_{\mathbf{j}}^{'}\widetilde{\boldsymbol{\omega}}_{\mathbf{j}}^{'}\right)\ \mathbf{s}_{\mathbf{j}}^{'\mathbf{P}} \tag{A26}$$

Jounce RHS $\boldsymbol{\sigma}^{\mathbf{s}}$ for a spherical joint must conform to (8) as shown in (A27). The first time derivative of the jerk RHS is provided in (A28-A29). Generalized jerks for a spherical joint are shown in (A30) and their product with Jacobian terms is shown in (A31). Partial derivatives with respect to generalized coordinates are shown in (A32) and the final product with generalized velocities is provided in (A33). Substituting into (A27) provides jounce RHS $\boldsymbol{\sigma}^{\mathbf{s}}$ in (A34) which matches (82).

$$\boldsymbol{\sigma}^{\mathbf{s}} = \dot{\boldsymbol{\eta}}^{s} - \left(\Phi^{\mathbf{s}}_{\mathbf{q}}\dddot{\mathbf{q}}\right)_{\mathbf{q}}\dot{\mathbf{q}} \tag{A27}$$

$$\dot{\boldsymbol{\eta}} = \mathbf{A}_i(\dot{\mathbf{H}}_i' + \tilde{\omega}_i'\mathbf{H}_i')\mathbf{s}_i^P - \mathbf{A}_j\left(\dot{\mathbf{H}}_j' + \tilde{\omega}_j'\mathbf{H}_i'\right)\mathbf{s}_j^P \tag{A28}$$

$$\dot{\mathbf{H}}_i' = \ddot{\tilde{\omega}}_i'\tilde{\omega}_i' + 3\dot{\tilde{\omega}}_i'\ddot{\tilde{\omega}}_i' + 2\tilde{\omega}_i'\ddot{\tilde{\omega}}_i' + \dot{\tilde{\omega}}_i'\tilde{\omega}_i'\tilde{\omega}_i' + \tilde{\omega}_i'\dot{\tilde{\omega}}_i'\tilde{\omega}_i' + \tilde{\omega}_i'\tilde{\omega}_i'\dot{\tilde{\omega}}_i' \tag{A29}$$

$$\dddot{\mathbf{q}}_i = \begin{Bmatrix} \dddot{\mathbf{r}}_i \\ \ddot{\boldsymbol{\omega}}_i' \end{Bmatrix} \qquad \dddot{\mathbf{q}}_j = \begin{Bmatrix} \dddot{\mathbf{r}}_j \\ \ddot{\boldsymbol{\omega}}_j' \end{Bmatrix} \tag{A30}$$

$$\boldsymbol{\Phi}_q\dddot{\mathbf{q}} = -\dddot{\mathbf{r}}_i - \mathbf{A}_i\ddot{\tilde{\omega}}_i'\mathbf{s}_i'^P + \dddot{\mathbf{r}}_j + \mathbf{A}_j\ddot{\tilde{\omega}}_j'\mathbf{s}_j'^P \tag{A31}$$

$$\begin{aligned} \left(\Phi_q\dddot{\mathbf{q}}\right)_{ri} &= \mathbf{0}_{3x3} \qquad \left(\Phi_q\dddot{\mathbf{q}}\right)_{\pi i'} = \mathbf{A}_i\left(\ddot{\tilde{\omega}}_i'\tilde{\mathbf{s}}_i'^P - \tilde{\mathbf{s}}_i'^P\ddot{\tilde{\omega}}_i'\right) \\ \left(\Phi_q\dddot{\mathbf{q}}\right)_{rj} &= \mathbf{0}_{3x3} \qquad \left(\Phi_q\dddot{\mathbf{q}}\right)_{\pi j'} = -\mathbf{A}_j\left(\ddot{\tilde{\omega}}_j'\tilde{\mathbf{s}}_j'^P - \tilde{\mathbf{s}}_j'^P\ddot{\tilde{\omega}}_j'\right) \end{aligned} \tag{A32}$$

$$\left(\Phi_q\dddot{\mathbf{q}}\right)_q\dot{\mathbf{q}} = \mathbf{A}_j\tilde{\omega}_j'\ddot{\tilde{\omega}}_j'\mathbf{s}_j'^P - \mathbf{A}_i\tilde{\omega}_i'\ddot{\tilde{\omega}}_i'\mathbf{s}_i'^P \tag{A33}$$

$$\begin{aligned} \boldsymbol{\sigma}^s = \mathbf{A}_i\Big(&\ddot{\tilde{\omega}}_i'\tilde{\omega}_i' + 3\dot{\tilde{\omega}}_i'\ddot{\tilde{\omega}}_i' + \dddot{\tilde{\omega}}_i'\tilde{\omega}_i' + 3\tilde{\omega}_i'\ddot{\tilde{\omega}}_i' + \dot{\tilde{\omega}}_i'\tilde{\omega}_i'\tilde{\omega}_i' + 2\tilde{\omega}_i'\dot{\tilde{\omega}}_i'\tilde{\omega}_i' + 3\tilde{\omega}_i'\tilde{\omega}_i'\dot{\tilde{\omega}}_i' + \tilde{\omega}_i'\tilde{\omega}_i'\tilde{\omega}_i'\tilde{\omega}_i'\Big)\mathbf{s}_i'^P \\ -\mathbf{A}_j\Big(&\ddot{\tilde{\omega}}_j'\tilde{\omega}_j' + 3\dot{\tilde{\omega}}_j'\ddot{\tilde{\omega}}_j' + 3\tilde{\omega}_j'\ddot{\tilde{\omega}}_j' + \dot{\tilde{\omega}}_j'\tilde{\omega}_j'\tilde{\omega}_j' + 2\tilde{\omega}_j'\dot{\tilde{\omega}}_j'\tilde{\omega}_j' + 3\tilde{\omega}_j'\tilde{\omega}_j'\dot{\tilde{\omega}}_j' + \tilde{\omega}_j'\tilde{\omega}_j'\tilde{\omega}_j'\tilde{\omega}_j'\Big)\mathbf{s}_j'^P \end{aligned} \tag{A34}$$

Appendix B. - Nomenclature

general vector/matrix dimensions

- *nb* = number of moving bodies
- *nc* = number of constraints (*nc*=*nk*+*nd*)
- *nd* = number of kinematic driver constraints
- *nk* = number of kinematic joint constraints
- *nq* = number of generalized coordinates (*nq*=3 *nb* planar, *nq*=6 *nb* spatial)

subscripts

- i = subscript denoting body i
- j = subscript denoting body j
- k = subscript for sample index within discretized sequence (see u_k)
- m = subscript denoting body m
- q = subscript denoting partial derivatives with respect to all generalized coordinates **q**
- qi = subscript denoting partial derivatives with respect to generalized coordinates for only body i
- qj = subscript denoting partial derivatives with respect to generalized coordinates for only body j
- qm = subscript denoting partial derivatives with respect to generalized coordinates for only body m
- ri = subscript denoting partial derivatives with respect to $\mathbf{r}_i$ location of body i
- $\pi i'$ = subscript denoting partial derivatives with respect to π_i' body-fixed directions for body i
- t = subscript denoting partial derivative with respect to time
- x = subscript for x coordinate component
- y = subscript for y coordinate component
- z = subscript for z coordinate component

General superscripts

- P = superscript for point P
- Q = superscript for point Q
- ( )′ = prime symbol denotes local body-fixed coordinate directions

Superscripts for joint/driver constraints

dri = general kinematic driver constraint
d1 = spatial dot-1 kinematic constraint
d2 = spatial dot-2 kinematic constraint
d2dd = spatial dot-2 distance driver constraint
frrd = spatial fixed revolute rotation driver constraint
jnt = general kinematic joint constraint
pp1 = planar parallel-1 kinematic constraint
pp2 = planar parallel-2 kinematic constraint
pp2dd = planar parallel-2 distance driver constraint
prdd = planar relative distance driver constraint
r = planar revolute kinematic joint constraint
rcd = planar relative coordinate driver constraint
rgr = planar relative gear ratio driver constraint
rr = planar double-revolute kinematic joint constraint
roll = planar rolling along line driver constraint
s = spatial spherical kinematic joint constraint
ss = spatial double-spherical kinematic joint constraint
srdd = spatial relative distance driver constraint

Scalars

C = general constant
K = general constant
L = constant length
d = distance BD for revolute-spherical-prismatic-universal (RSPU) mechanism f(t) = function of time
h = constant time step Δt
t = time
u_k = sample k of variable u discretized at equal intervals h
θ = rotation angle
ρ = rolling radius of wheel or pitch radius of gear
τ = time period of oscillation for sinusoidal driver
ψ = output rotation angle
ϕ_i = orientation angle for body i (planar only)
$\dot{\phi}_i$ = angular velocity for body i (planar only)
$\ddot{\phi}_i$ = angular acceleration for body i (planar only)
$\dddot{\phi}_i$ = angular jerk for body i (planar only)
$\ddddot{\phi}_i$ = angular jounce for body i (planar only)

Column vectors

$\mathbf{a_i}$ = location of point Q on body i relative to point P on body i measured in global directions (2×1 planar, 3×1 spatial)
$\mathbf{a_i'}$ = location of point Q on body i relative to point P on body i measured in local body-fixed directions (2×1 planar, 3×1 spatial)
$\mathbf{d_{ij}}$ = location of point P on body j relative to point P on body i measured in global directions (2×1 planar, 3×1 spatial)
$\mathbf{p_i}$ = Euler parameter unit quaternion describing attitude of body i (4×1 spatial)
$\mathbf{q}$ = all generalized coordinates ($nq \times 1$)
$\dot{\mathbf{q}}$ = all generalized velocities ($nq \times 1$)
$\ddot{\mathbf{q}}$ = all generalized accelerations ($nq \times 1$)
$\dddot{\mathbf{q}}$ = all generalized jerks ($nq \times 1$)
$\ddddot{\mathbf{q}}$ = all generalized jounces ($nq \times 1$)
$\mathbf{q_i}$ = generalized coordinates for body i (3×1 planar, 6×1 spatial)
$\mathbf{r_i}$ = global location of frame attached to body i (2×1 planar, 3×1 spatial)
$\dot{\mathbf{r}}_\mathbf{i}$ = velocity of frame attached to body i (2×1 planar, 3×1 spatial)
$\ddot{\mathbf{r}}_\mathbf{i}$ = acceleration of frame attached to body i (2×1 planar, 3×1 spatial)
$\dddot{\mathbf{r}}_\mathbf{i}$ = jerk of frame attached to body i (2×1 planar, 3×1 spatial)
$\ddddot{\mathbf{r}}_\mathbf{i}$ = jounce of frame attached to body i (2×1 planar, 3×1 spatial)

$\mathbf{r_i^P}$ = global location of point P attached to body i (*2 × 1* planar, *3 × 1* spatial)
$\mathbf{s_i'^P}$ = constant location of point P on body i relative to frame attached to body i measured in local body-fixed directions (*2 × 1* planar, *3 × 1* spatial)
$\hat{\mathbf{u}}$ = unit vector along fixed axis of revolute rotation driver (*3 × 1* spatial)
$\mathbf{\Phi}$ = all joint and driver constraints (*nc x 1*)
$\boldsymbol{\gamma}$ = all acceleration right-hand-side terms (*nc x 1*)
$\boldsymbol{\eta}$ = all jerk right-hand-side terms (*nc x 1*)
$\boldsymbol{\nu}$ = all velocity right-hand-side terms (*nc x 1*)
$\boldsymbol{\sigma}$ = all jounce right-hand-side terms (*nc x 1*)
$\boldsymbol{\omega_i}$ = angular velocity for body i measured in global directions (*3 × 1* spatial)
$\boldsymbol{\omega_i'}$ = angular velocity for body i measured in local body-fixed directions (*3 × 1* spatial)
$\dot{\boldsymbol{\omega}}_\mathbf{i}'$ = angular acceleration for body i measured in local body-fixed directions (*3 × 1* spatial)
$\ddot{\boldsymbol{\omega}}_\mathbf{i}'$ = angular jerk for body i measured in local body-fixed directions (*3 × 1* spatial)
$\dddot{\boldsymbol{\omega}}_\mathbf{i}'$ = angular jounce for body i measured in local body-fixed directions (*3 × 1* spatial)

Matrices

$\mathbf{A_i}$ = attitude matrix for body i (*2 × 2* planar, *3 × 3* spatial)
$\mathbf{B_i}$ = second attitude matrix for body i (*2 × 2* planar)
$\mathbf{H_i'}$ = angular jerk product matrix for body i using components in local body-fixed directions (*3 × 3* spatial)
$\mathbf{I_2}$ = *2 × 2* identity matrix
$\mathbf{I_3}$ = *3 × 3* identity matrix
$\mathbf{R}$ = constant orthogonal rotator matrix (*2 × 2* planar)
$\mathbf{W_i'}$ = angular jounce product matrix for body i using components in local body-fixed directions (*3 × 3* spatial)
$\mathbf{\Phi_q}$ = Jacobian matrix containing partial derivatives of constraints $\mathbf{\Phi}$ with respect to generalized coordinates $\mathbf{q}$(*nc x nq)*
$\widetilde{\boldsymbol{\omega}}_\mathbf{i}'$ = skew-symmetric angular velocity matrix for body i using components in local body-fixed directions (*3 × 3* spatial)
$\dot{\widetilde{\boldsymbol{\omega}}}_\mathbf{i}'$ = skew-symmetric angular acceleration matrix for body i using components in local body-fixed directions (*3 × 3* spatial)
$\ddot{\widetilde{\boldsymbol{\omega}}}_\mathbf{i}'$ = skew-symmetric angular jerk matrix for body i using components in local body-fixed directions (*3 × 3* spatial)
$\dddot{\widetilde{\boldsymbol{\omega}}}_\mathbf{i}$ = skew-symmetric angular jounce matrix for body i using components in local body-fixed directions (*3 × 3* spatial)
$\mathbf{0_{2x2}}$ = *2 × 2* zero matrix
$\mathbf{0_{3x3}}$ = *3 × 3* zero matrix

Vector/Matrix operations

$\mathbf{e^T}$ = vector transpose for $\mathbf{e}$
$\mathbf{E^T}$ = matrix transpose for $\mathbf{E}$
$\widetilde{\mathbf{e}}$ = skew-symmetric operator $\widetilde{\mathbf{e}} = \begin{bmatrix} 0 & -e_3 & e_2 \\ e_3 & 0 & -e_1 \\ -e_2 & e_1 & 0 \end{bmatrix}$ for $\mathbf{e} = \begin{Bmatrix} e_1 \\ e_2 \\ e_3 \end{Bmatrix}$

References

[1] H. Hayati, D. Eager, A.M. Pendrill, H Alberg, Jerk within the context of science and engineering - a systematic review, Vibration. 3 (4) (2020) 371–409, https://doi.org/10.3390/vibration3040025.
[2] H.A. Rothbart, Cams: Design, Dynamics, and Accuracy, John Wiley, 1956. ISBN 978-0471739531.
[3] Y.S. Lu, Y.Y. Lin, Smooth motion control of rigid robotic manipulators with constraints on high-order kinematic variables, Mechatronics 49 (2018) 11–25, https://doi.org/10.1016/j.mechatronics.2017.11.003.
[4] D. Chen, S. Li, W. Li, Q. Wu, A multi-level simultaneous minimization scheme applied to jerk-bounded redundant robot manipulators, IEEE Trans. Automat. Sci. Eng. 17 (1) (2020) 463–474, https://doi.org/10.1109/TASE.2019.2931810.
[5] Y. Fang, J. Qi, J. Hu, W. Wang, Y. Peng, An approach for jerk-continuous trajectory generation of robotic manipulators with kinematical constraints, Mechanism and machine theory 153 (2020) 103957, https://doi.org/10.1016/j.mechmachtheory.2020.103957.
[6] B. Alpers, On fast jerk-continuous motion functions with higher-order kinematic restrictions for online trajectory generation, Robotics 11 (4) (2022) 73, https://doi.org/10.3390/robotics11040073.
[7] X. Li, X. Gao, W. Zhang, L. Hao, Smooth and collision-free trajectory generation in cluttered environments using cubic B-spline form, Mech. Mach. Theory 169 (2022) 104606, https://doi.org/10.1016/j.mechmachtheory.2021.104606.
[8] D. Stretti, P. Fanghella, G. Berselli, L. Bruzzone, Analytical expression of motion profiles with elliptic jerk, Robotica 41 (7) (2023) 1976–1990, https://doi.org/10.1017/S0263574723000255.
[9] Z. Wu, J. Chen, D. Zhang, J. Wang, L. Zhang, F. Xu, A novel multi-point trajectory generator for robotic manipulators based on piecewise motion profile and series-parallel analytical strategy, Mech. Mach. Theory 181 (2023) 105201, https://doi.org/10.1016/j.mechmachtheory.2022.105201.

[10] B. Sencer, S. Tajima, Frequency optimal feed motion planning in computer numerical controlled machine tools for vibration avoidance, ASME J. Manuf. Sci. Eng. 139 (1) (2017) 011006, https://doi.org/10.1115/1.4034140.

[11] L. Zhang, J. Du, Acceleration smoothing algorithm based on jounce limited for corner motion in high-speed machining, Int. J. Adv. Manuf. Technol. 95 (2018) 1487–1504, https://doi.org/10.1007/s00170-017-1272-3.

[12] L. Chanda, R.J. Cripps, Characterising the effects of shape on tool path motion, Int. J. Mach. Tool. Manuf. 132 (2018) 17–35, https://doi.org/10.1016/j.ijmachtools.2018.04.005.

[13] H. Li, J. Rastegar, B. Wang, W. Wu, Z Yan, A corner smoothing algorithm using trajectory pattern method (TPM) for high-speed and high-quality machining, Adv. Mech. Eng. 13 (8) (2021), https://doi.org/10.1177/16878140211040671.

[14] D. Mellinger, V. Kumar, Minimum snap trajectory generation and control for quadrotors, in: 2011 IEEE International conference on robotics and automation, 2011, pp. 2520–2525, https://doi.org/10.1109/ICRA.2011.5980409.

[15] J. Mooney, E.N Johnson, Efficient approximation of optimal high-order kinematic trajectories, in: 2016 AIAA Guidance, navigation, and control conference, 2016, p. 2016, https://doi.org/10.2514/6.2016-1870. -1870.

[16] M.M. de Almeida, M. Akella, New numerically stable solutions for minimum-snap quadcopter aggressive maneuvers, in: 2017 American control conference, 2017, pp. 1322–1327, https://doi.org/10.23919/ACC.2017.7963135.

[17] Z. Ma, H. Qiu, H. Wang, L. Yang, L. Huang, R. Qiu, A* algorithm path planning and minimum snap trajectory generation for mobile robot, in: IEEE 4th International conference on robotics, control and automation engineering, 2021, pp. 284–288, https://doi.org/10.1109/RCAE53607.2021.9638900.

[18] X. Zhao, K. Wang, S. Wu, L. Wen, Z. Chen, L. Dong, C. Wu, An obstacle avoidance path planner for an autonomous tractor using the minimum snap algorithm, Comput. Electron. Agric. 207 (2023) 107738, https://doi.org/10.1016/j.compag.2023.107738.

[19] T. Flash, N. Hogan, The coordination of arm movements: an experimentally confirmed mathematical model, J. Neurosci. 5 (7) (1985) 1688–1703, https://doi.org/10.1523/JNEUROSCI.05-07-01688.1985.

[20] J. Laczko, R.A. Scheidt, L.S. Simo, D Piovesan, Inter-joint coordination deficits revealed in the decomposition of endpoint jerk during goal-directed arm movement after stroke, IEEE Trans. Neural Syst. Rehabilit. Eng. 25 (7) (2017) 798–810, https://doi.org/10.1109/TNSRE.2017.2652393.

[21] D.S. de Lucena, O. Stoller, J.B. Rowe, V. Chan, D.J. Reinkensmeyer, Wearable sensing for rehabilitation after stroke: bimanual jerk asymmetry encodes unique information about the variability of upper extremity recovery, in: 2017 International conference on rehabilitation robotics, 2017, pp. 1603–1608, https://doi.org/10.1109/ICORR.2017.8009477.

[22] L. Zhang, M.M. Diraneyya, J. Ryu, C.T. Haas, E.M Abdel-Rahman, Jerk as an indicator of physical exertion and fatigue, Autom. Constr. 104 (2019) 120–128, https://doi.org/10.1016/j.autcon.2019.04.016.

[23] S. Edelman, T. Flash, A model of handwriting, Biol. Cybern. 57 (1–2) (1987) 25–36, https://doi.org/10.1007/BF00318713.

[24] K.E. Novak, L.E. Miller, J.C. Houk, Kinematic properties of rapid hand movements in a knob turning task, Exp. Brain Res. 132 (2000) 419–433, https://doi.org/10.1007/s002210000366.

[25] K. Saho, K. Sugano, M. Kita, K. Uemura, M. Matsumoto, Classification of health literacy and cognitive impairments using higher-order kinematic parameters of the sit-to-stand movement from a monostatic Doppler radar, IEEE Sens. J. 21 (8) (2021) 10183–10192, https://doi.org/10.1109/JSEN.2021.3060050.

[26] P.D. Sparis, S.G. Mouroutsos, A new matrix method for the kinematic analysis and motion simulation of planar mechanisms with lower pairs, ASME J. Mech. Transm. Automatic Design 106 (4) (1984) 429–436, https://doi.org/10.1115/1.3258590.

[27] G. Figliolini, C Lanni, Jerk and jounce relevance for the kinematic performance of long-dwell mechanisms, in: Advances in mechanism and machine science: proceedings of the 15th IFTOMM world congress on mechanism and machine science 15, Springer International Publishing, 2019, pp. 219–228, https://doi.org/10.1007/978-3-030-20131-9_22.

[28] J.M. Rico, J. Gallardo, J. Duffy, Screw theory and higher order kinematic analysis of open serial and closed chains, Mech. Mach. Theory 34 (4) (1999) 559–586, https://doi.org/10.1016/S0094-114X(98)00029-9.

[29] J. Gallardo-Alvarado, J.M. Rico-Martinez, Jerk influence coefficients, via screw theory, of closed chains, Meccanica 36 (2001) 213–228, https://doi.org/10.1023/A:1013074907533.

[30] J. Gallardo-Alvarado, Hyper-jerk analysis of robot manipulators, J. Intell. Robot. Syst. 74 (3–4) (2014) 625–641, https://doi.org/10.1007/s10846-013-9849-z.

[31] P.C. López-Custodio, J.M. Rico, J.J. Cervantes-Sánchez, G.I. Pérez-Soto, C.R. Díez-Martínez, Verification of the higher order kinematic analyses equations, Eur. J. Mech.-a/solids 61 (2017) 198–215, https://doi.org/10.1016/j.euromechsol.2016.09.010.

[32] A. Müller, An overview of formulae for the higher-order kinematics of lower-pair chains with applications in robotics and mechanism theory, Mech. Mach. Theory 142 (2019) 103594, https://doi.org/10.1016/j.mechmachtheory.2019.103594.

[33] Z. Fu, E. Spyrakos-Papastavridis, Y.H. Lin, J.S. Dai, Analytical expressions of serial manipulator Jacobians and their high-order derivatives based on lie theory, in: 2020 IEEE International conference on robotics and automation, 2020, pp. 7095–7100, https://doi.org/10.1109/ICRA40945.2020.9197131.

[34] D. Condurache, Higher-order relative kinematics of rigid body and multibody systems. a novel approach with real and dual lie algebras, Mech. Mach. Theory 176 (2022) 104999, https://doi.org/10.1016/j.mechmachtheory.2022.104999.

[35] D. Condurache, Higher-order kinematics of lower-pair chains with hyper-multidual algebra, in: ASME International design engineering technical conferences and computers and information in engineering conference, 2022, p. 86281, https://doi.org/10.1115/DETC2022-88781. V007T07A073.

[36] R. Peón-Escalante, A. Espinosa-Romero, F. Peñuñuri, Higher order kinematic formulas and its numerical computation employing dual numbers, Mech. Based Design Struct. Mach. (2023) 1–16, https://doi.org/10.1080/15397734.2023.2203220.

[37] R. Di Gregorio, Acceleration and higher-order analyses solved by extending the superposition principle: the incipient motion technique, Mech. Mach. Theory 153 (2020) 103953, https://doi.org/10.1016/j.mechmachtheory.2020.103953.

[38] H.J. Sommer, Jerk analysis and axode geometry of spatial linkages, ASME J. Mech. Design 130 (4) (2008) 42301, https://doi.org/10.1115/1.2838323.

[39] C.G. Lo Bianco, Evaluation of generalized force derivatives by means of a recursive Newton–Euler approach, IEEE Trans. Robot. 25 (4) (2009) 954–959, https://doi.org/10.1109/TRO.2009.2024787.

[40] F. Urbinati, E. Pennestrì, A tool for third order kinematic analysis of spatial mechanisms, in: ASME International design engineering technical conferences and computers and information in engineering conference, 1998, p. 80319, https://doi.org/10.1115/DETC98/MECH-5901. V01BT01A082.

[41] E.J. Haug, Computer Aided Kinematics and Dynamics of Mechanical Systems, 1, Allyn and Bacon, 1989. ISBN 978-0205116690.

[42] D.C. Lin, C.P. McGowan, K.P. Blum, L.H. Ting, Yank: the time derivative of force is an important biomechanical variable in sensorimotor systems, J. Exp. Biol. 222 (18) (2019) jeb180414, https://doi.org/10.1242/jeb.180414.

[43] E.A. Baran, T. Uzunovic, A. Sabanovic, Performance improvement of bilateral control systems using derivative of force, Robotica 36 (11) (2018) 1627–1640, https://doi.org/10.1017/S0263574718000607.

[44] K. Yang, W. Yang, C Wang, Inverse dynamic analysis and position error evaluation of the heavy-duty industrial robot with elastic joints: an efficient approach based on Lie group, Nonlinear Dyn. 93 (2018) 487–504, https://doi.org/10.1007/s11071-018-4205-2.

[45] H.J. Sommer, Third-order differential-algebraic equations for improved integration of multibody dynamics, in: ASME International design engineering technical conferences and computers and information in engineering conference, 2017, https://doi.org/10.1115/DETC2017-67448. *DETC2017-67448*, V006T10A003.

[46] C.G. Lo Bianco, O. Gerelli, Online trajectory scaling for manipulators subject to high-order kinematic and dynamic constraints, IEEE Trans. Robot. 27 (6) (2011) 1144–1152, https://doi.org/10.1109/TRO.2011.2162268.

[47] D. Kaserer, H. Gattringer, A. Müller, Nearly optimal path following with jerk and torque rate limits using dynamic programming, IEEE Trans. Robot. 35 (2) (2018) 521–528, https://doi.org/10.1109/TRO.2018.2880120.

[48] A. Müller, S. Kumar, Closed-form time derivatives of the equations of motion of rigid body systems, Multibody Syst. Dyn. 53 (3) (2021) 257–273, https://doi.org/10.1007/s11044-021-09796-8.

[49] A. Müller, S. Kumar, T. Kordik, A recursive lie-group formulation for the second-order time derivatives of the inverse dynamics of parallel kinematic manipulators, IEEe Robot. Autom. Lett. 8 (6) (2023) 3804–3811, https://doi.org/10.1109/LRA.2023.3267005.
[50] MATLAB, Version 9.7.0.1247435 (R2019b), MathWorks, Natick, MA, 2019.
[51] B. Fornberg, Generation of finite difference formulas on arbitrarily spaced grids, Math. Comput. 51 (184) (1988) 699–706, https://doi.org/10.1090/S0025-5718-1988-0935077-0.